Effect of micro-grooved surface on the static and dynamic characteristics of journal bearings with misalignment

Peng Li[1], Zhanqun Shi[1], Hao Zhang[1], Xin Li[2], Sen Xiao[1] and Fengshou Gu[3]

[1]Tianjin Key Laboratory of Power Transmission and Safety Technology for New Energy Vehicles, School of Mechanical Engineering, Hebei University of Technology, Tianjin 300401, China

[2]China North Engine Research Institute, Tianjin 300400, China

[3]Centre for Efficiency and Performance Engineering, University of Huddersfield, Huddersfield HD1 3DH, UK

Corresponding author: Hao Zhang (E-mail: zhanghao@hebut.edu.cn)

Abstract

This paper presents a hydrodynamic lubrication model to investigate the static and dynamic characteristics of micro-grooved bearings considering journal misalignment. An averaged Reynolds equation with the mass conservation is derived and numerical procedure is solved by the finite difference method. The influences of eccentricity ratio, misalignment and micro-groove parameters on lubrication performances of aligned/misaligned journal bearings are compared systematically. Mathematical expressions of five micro-grooves with different geometric shapes i.e., straight-groove, left spiral-groove, right spiral-groove, left herringbone-groove and right herringbone-groove are given. The results show that with the increase of degree of misalignment, the load carrying capacity, main stiffness and damping coefficients increase, and the friction coefficient decreases, while the effect of misalignment angle on bearing performance is opposite. The results also indicated that the left herringbone-groove has better performance improvement for aligned journal bearing, while the right spiral-groove has better performance improvement for misaligned journal bearing under the optimal micro-groove parameters, especially at low eccentricity ratio. Moreover, the amount of the performance improvement of micro-grooved bearing depends on the design of the micro-groove parameters. This study can provide theoretical guidance for the design optimization of micro-grooved journal bearings with misalignment.

Keywords

Static and dynamic characteristics, micro-groove, misalignment, averaged Reynolds equation, journal bearing.

1. Introduction

Misalignment is one of the most common faults for journal bearings due to manufacturing and installation errors, shaft deformation, etc. The fluid film provides support force for the shaft and avoids surface wear caused by the direct contact between the journal and bearing, the change of the fluid film thickness induced by misalignment leads to the asymmetric distribution of fluid pressure that deteriorates the lubrication performance.[1,2] If the degree of misalignment exceeds a certain threshold, the contact may occur between solid surfaces, and then wear will affect the lubrication performance of bearing.[3,4] Hence, it is of great significance to study the effects of misalignment on lubrication performance of journal bearing systems.

MaKee and McKee[5] firstly analyzed the effect of journal misalignment on the maximum fluid pressure in the axial direction. Subsequently, DuBois et al.[6] found that journal misalignment can give rise to the asymmetric distribution of fluid film pressure. Sun and Gui[7,8] derived the fluid film thickness expression for misaligned journal bearings and pointed

out that journal misalignment resulted in an increase in the maximum fluid pressure and a decrease in the fluid film thickness. Lv et al.[9] proposed an approach to analyze the equivalent supporting point location as well as load carrying capacity of vertically misaligned journal bearings. Recently, Feng et al.[10] compared the static and dynamic performance parameters of aligned and misaligned bearings considering the effects of turbulent flow and thermal hydrodynamics. Zheng et al.[11] studied the effects of couple stress lubricant on the static performance of misaligned journal bearings and stated that the load-carrying capacity can be improved when the values of couple stress parameter and eccentricity are larger. It was concluded that with a large degree of misalignment, the elastic deformation of journal bearing cannot be ignored. El-Butch and Ashour[12] presented a numerical study for misaligned elastic tilting-pad journal bearings and found that the misalignment reduced film thickness and the thermoelastic deformation increased film thickness could balance each other at lower degree of journal misalignment. Wang et al.[13] concluded that journal misalignment leads to the occurrence of elastic deformation and stated that the deformation magnitude of bearing decreases with the misalignment angle increases.

As misalignment reaches a large degree, the minimum fluid film thickness reduces to the same order of surface roughness, and thus the effects of surface roughness on the performance of journal bearings cannot be neglected. In such cases, incorporating surface roughness into the analytical model will yield more accurate results. Guha et al.[14] clarified that the misalignment angle significantly affected the friction coefficient of journal bearings and the misalignment moment decreases as the roughness increases. Meng et al.[15] improved the average flow model and asperity contact model by considering elastic deformation of rough surfaces[16,17], inter-asperity cavitation, and lubricant thermal effects[18]. Lv et al.[19,20] investigated the mixed lubrication performance of misaligned bearings considering wall slip and turbulence. The results showed that journal misalignment significantly reduces minimum film thickness and increases maximum film pressure, and the transition speed from mixed lubrication regime to hydrodynamic lubrication regime increases. Zhu et al.[21] analyzed the coupled effects of surface roughness and journal misalignment on the thermo-hydrodynamic lubrication performance of the bearing. Xie et al.[22] numerically and experimentally investigated the effects of misalignment on the static and dynamic performance of water-lubricated bearings taking surface roughness and thermal effects into account. Ma et al.[23] explored the effect of journal misalignment and non-Gaussian rough surfaces on the static performance of journal bearings. Sahu et al.[24] numerically analyzed the influences of journal misalignment and surface irregularities on magnetorheological fluid journal bearings and found that the occurrence of misalignment increased the fluid film damping coefficient and friction torque.

Recently, surface texture technique is found to be an effective way to improve the performance of journal bearing and prevent bearing wear induced by excessive misalignment. The surface texture acts as a set of micro-bearings that provides an additional hydrodynamic effect.[25] Micro-groove is the most popular type of surface texture because it is much easier to be machined in comparison with others. Adatepe et al.[26,27] experimentally analyzed the tribological performance of micro-grooved journal bearings and made an optimization on the shape of micro-grooves. Kango et al.[28] compared the lubrication performance between various textured journal bearings and found that micro-grooved surface significantly reduced the friction coefficient of bearing. The effects of micro-groove on dynamic coefficients i.e., stiffness and damping coefficients were investigated by Miyanaga and Tomioka[29]. Gong et al.[30] numerically analyzed the lubrication performance of micro-grooved water-lubricated journal bearings and pointed out that the optimal depth of the micro-groove is different for different bearing materials. Xiang et al.[31,32] studied the tribo-dynamic performances during start-up of water-lubricated bearings considering micro-groove bottom shape and imperfect

journal. Subsequently, the same group[33,34] further analyzed the nonlinear dynamic mixed friction behaviors and tribo-dynamic responses of water-lubricated bearings under different geometric parameters. Xie et al.[35] numerically and experimentally investigated the fluid-structure interaction behaviors of the axial asymmetric micro-grooved bearing. It was found that the maximum fluid film pressure and load carrying capacity was improved due to the increased hydrodynamic effects. The optimization of micro-groove in terms of load carrying capacity and friction coefficient via a variety of multi-objective optimization algorithms was studied by a number of researchers.[36,37] However, to the authors' knowledge, comprehensive research that analyze the effect of journal misalignment and micro-grooved surfaces on the static and dynamic characteristics of bearings are still limited, especially for the analysis on the optimal geometric parameters of micro-groove in misaligned journal bearings.

The objective of this paper is to study the lubrication characteristics of micro-grooved bearings under different analytical parameters with consideration of journal misalignment. To achieve this objective, a modified Reynolds equation with the mass conservation boundary condition will be developed. The influences of eccentricity ratio, degree of misalignment, misalignment angle, micro-groove geometric shape, deflection angle and depth on lubrication performances of journal bearings will be investigated systematically. In addition, the lubrication characteristics of micro-grooved bearings between models with and without misalignment are analyzed comparatively.

The content of the remainder of this study is described as follows. The theoretical mechanisms related to the lubrication performances are established, and the mathematical models of misalignment and micro-groove are given in Section 2. The detailed flow of the global solution is given in Section 3. The effects of eccentricity ratio, degree of misalignment, misalignment angle and micro-groove parameters (deflection angle and depth) on static and dynamic characteristics are systemically investigated by numerical simulation in Section 4. Finally, the results are discussed and theoretical guidance for the design optimization of misaligned and micro-grooved bearings is provided.

2. Mathematical model

The schematic diagram of misaligned and micro-grooved journal bearing with different surface scales is shown in **Figure 1**. The front and side views of journal bearing are respectively shown in **Figure 1(a)** and **(b)**. The contact states of journal and bearing at different surface scales (global scale, micro-groove scale and roughness scale) are given in **Figure 1(c)**.

2.1. Average Reynolds equation

The fluid film is assumed as steady state, incompressible, isothermal, laminar, isoviscous, Newtonian fluid. According to the average Reynolds equation proposed by Patir and Cheng[38,39] and contact factor[40]. Fluid film cavitation phenomenon should be considered through the mass conservation cavitation model with rupture and reformation of the fluid film.[41] The average Reynolds equation with cavitation model can be expressed as follows:

$$\frac{\partial}{\partial x}\left(\phi_x \frac{\rho h^3}{\mu}\frac{\partial p}{\partial x}\right)+\frac{\partial}{\partial z}\left(\phi_z \frac{\rho h^3}{\mu}\frac{\partial p}{\partial z}\right)=6u\left(\phi_c \frac{\partial(\rho h\Theta)}{\partial x}+\sigma\frac{\partial(\rho\phi_s\Theta)}{\partial x}\right)+12\phi_c\frac{\partial(\rho h\Theta)}{\partial t} \tag{1}$$

Based on the mass balance of each node with uniquely defined fluxes, $p-\Theta$ cavitation model automatically satisfies the conditions of mass conservation throughout the lubricated area, the constraints conditions for cavitation are given as follows:[42,43]

$$\begin{cases} p > p_{cav} & \Rightarrow \Theta = 1 \ (\text{active region}) \\ 0 \le \Theta < 1 \Rightarrow p = p_{cav} & (\text{cavitation region}) \end{cases} \tag{2}$$

where ϕ_x and ϕ_z represent the pressure flow factors in the x and y directions and ϕ_s represent shear flow factor, respectively. ϕ_c represents the contact factor. $\sigma=\sqrt{\sigma_j^2+\sigma_b^2}$ represents the standard deviation of combined surface roughness of journal σ_j and bearing σ_b. u represents the linear velocity of journal. ρ and μ denote the fluid density and viscosity, respectively. p and h denote the fluid film pressure and film thickness, respectively. Θ represents the cavitation fraction, and t represents time. x, y, z represent coordinate system of bearing.

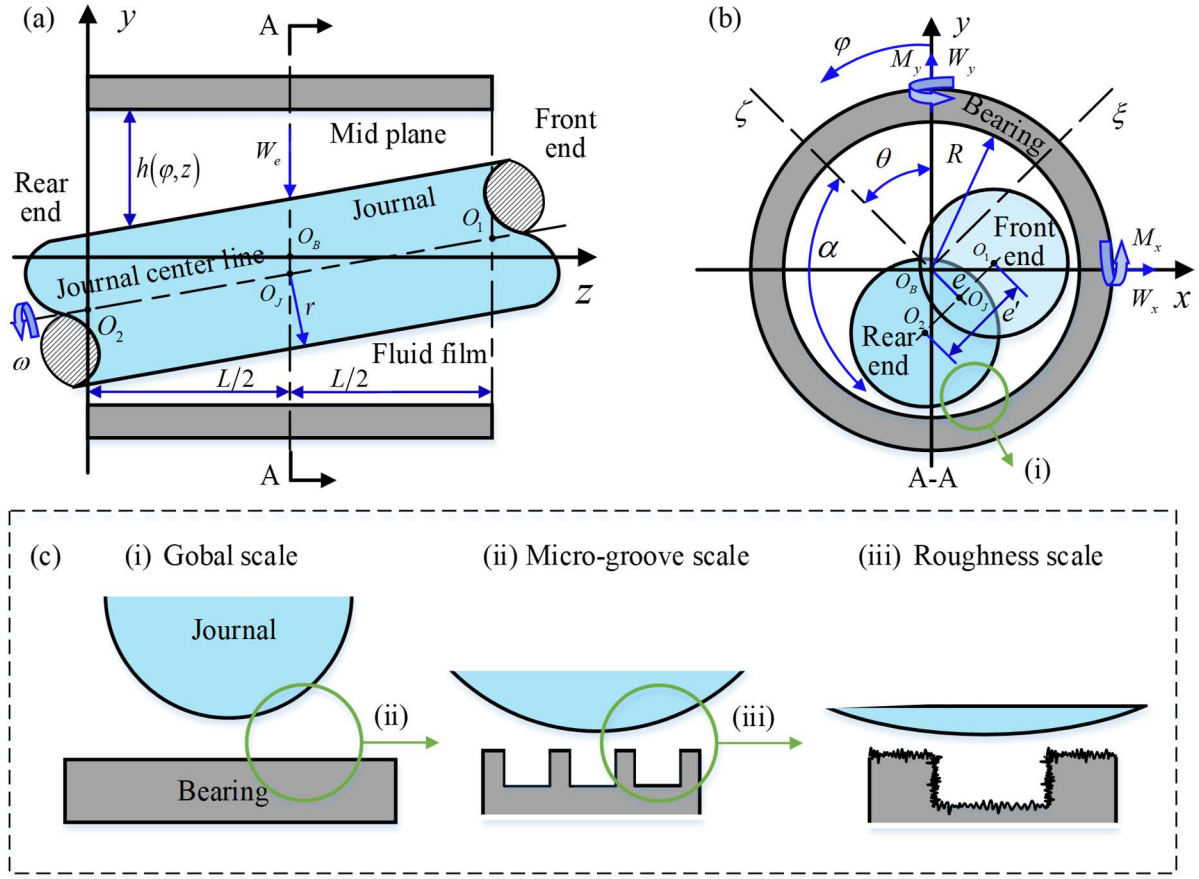

Figure 1. The schematic diagram of misaligned micro-grooved journal bearing with different surface scales: (a) and (b) the front and side views of the journal bearing; (c) the contact states of journal and bearing at different surface scales (global scale, micro-groove scale and roughness scale).

The dimensionless parameters are defined as follows:

$$\bar{h}=\frac{h}{c},\ \varepsilon=\frac{e}{c},\ \varepsilon'=\frac{e'}{c},\ \varphi=\frac{x}{R},\ Z=\frac{z}{L},\ \bar{u}=\frac{u}{U},\ \bar{p}=\frac{pc^2}{\mu UR},\ \bar{t}=\frac{Ut}{R} \tag{3}$$

where c represents the bearing radial clearance, $c=R-r$, R and r are the radius of bearing and journal, respectively, L represents the width of bearing. e and e' represent the eccentricity of the bearing mid-plane and the projected dimension of the misaligned journal on the midplane of the bearing, respectively. ε and ε' represent the eccentricity ratio and misalignment eccentricity ratio, respectively. U represents the dimension value of journal rotation speed.

Substituting the dimensionless parameters in equation (3) into equations (1) and (2), the dimensionless forms of the average Reynolds equation are derived as follows:

$$\frac{\partial}{\partial\varphi}\left(\phi_x\bar{h}^3\frac{\partial\bar{p}}{\partial\varphi}\right)+\frac{\partial}{\partial Z}\left(\phi_z\bar{h}^3\frac{\partial\bar{p}}{\partial Z}\right)=6\bar{u}\left(\phi_c\frac{\partial\left(\bar{h}\Theta\right)}{\partial\varphi}+\bar{\sigma}\frac{\partial\left(\phi_s\Theta\right)}{\partial\varphi}\right)+12\phi_c\frac{\partial\left(\bar{h}\Theta\right)}{\partial\bar{t}} \tag{4}$$

and dimensionless constraint is given as follows:

$$\begin{cases}\bar{p}>0 \quad \Rightarrow\Theta=1\ \left(\text{active region}\right)\\ 0\le\Theta<1\Rightarrow\bar{p}=0\ \left(\text{cavitation region}\right)\end{cases} \tag{5}$$

The expression of pressure flow factors $\left(\phi_x,\phi_z\right)$ are listed below:

$$\phi_x=\begin{cases}1-\kappa_1 e^{-\kappa_2\left(\bar{h}/\bar{\sigma}\right)} & \text{if } \gamma\le 1\\ 1+\kappa_1\left(\bar{h}/\bar{\sigma}\right)^{-\kappa_2} & \text{if } \gamma>1\end{cases} \tag{6}$$

$$\phi_z\left(\bar{h}/\bar{\sigma},\gamma\right)=\phi_x\left(\bar{h}/\bar{\sigma},1/\gamma\right) \tag{7}$$

where κ_1 and κ_2 are defined as constants, and γ is expressed as the parameter for different roughness directions.

The shear flow factor ϕ_s is given as follows:

$$\phi_s=\bar{V}_{rj}\Phi_s\left(\bar{h}/\bar{\sigma},\gamma_j\right)-\bar{V}_{rb}\Phi_s\left(\bar{h}/\bar{\sigma},\gamma_b\right) \tag{8}$$

where $\bar{V}_{rj}$, $\bar{V}_{rb}$ and ϕ_s are represented as:

$$\bar{V}_{rj}=\left(\bar{\sigma}_j/\bar{\sigma}\right)^2;\ \ \bar{V}_{rb}=\left(\bar{\sigma}_b/\bar{\sigma}\right)^2=1-\bar{V}_{rj} \tag{9}$$

$$\Phi_s=\begin{cases}A_1\left(\bar{h}/\bar{\sigma}\right)^{\alpha 1}e^{-\alpha 2\left(\bar{h}/\bar{\sigma}\right)+\alpha 3\left(\bar{h}/\bar{\sigma}\right)^2} & \text{if } \left(\bar{h}/\bar{\sigma}\right)\le 5\\ A_2 e^{-0.25\left(\bar{h}/\bar{\sigma}\right)} & \text{if } \left(\bar{h}/\bar{\sigma}\right)>5\end{cases} \tag{10}$$

where A_1, A_2, α_1, α_2 and α_3 are the constants to be derived, which values can be chosen in references.[38,39]

The contact factor ϕ_c is defined as follows:[40]

$$\phi_c=\begin{cases}e^{-0.6912+0.78\left(\bar{h}/\bar{\sigma}\right)-0.304\left(\bar{h}/\bar{\sigma}\right)^2+0.0401\left(\bar{h}/\bar{\sigma}\right)^3} & \text{if } 0\le\left(\bar{h}/\bar{\sigma}\right)<3\\ 1 & \text{if } \left(\bar{h}/\bar{\sigma}\right)\ge 3\end{cases} \tag{11}$$

2.2. Asperity contact model

For the journal with a large degree of misalignment, the asperity contact between the solid surfaces may occur, and hence the journal bearing may be operating within a mixed lubrication regime. To accurately evaluate bearing performance when large misalignment leads to mixed lubrication, the asperity contact model proposed by Greenwood and Tripp[44] is introduced to calculate the contact pressure, which is expressed as follows:

$$p_{asp}=\frac{16\sqrt{2}\pi}{15}\left(\sigma\beta\eta\right)^2E^*\sqrt{\frac{\sigma}{\beta}}F_{2.5}\left(h/\sigma\right) \tag{12}$$

where σ represents the standard deviation of combined surface roughness, β and η represent the curvature radius and density of asperities, respectively. E^* denotes the composite elastic modulus of journal and bearing, which can be calculated as follows:

$$E^*=\left(\left(1-\upsilon_b^2\right)/E_b+\left(1-\upsilon_j^2\right)/E_j\right)^{-1} \tag{13}$$

where υ_b and E_b represent the Poisson ratio and elastic modulus of the bearing shell, υ_j and E_j represent those of the journal. $F_{2.5}\left(h/\sigma\right)$ denotes a statistical function related to the film thickness ratio, which is given is as follows:

$$F_{2.5}\left(\overline{h}/\overline{\sigma}\right)=\begin{cases}2.134\times10^{-4}\exp\left(3.804\ \mathrm{In}\left(4-\overline{h}/\overline{\sigma}\right)+1.34\ \left(\mathrm{In}\left(4-\overline{h}/\overline{\sigma}\right)\right)^2\right) & \text{if } \left(\overline{h}/\overline{\sigma}\right)\le 3.5\\ 1.12\times10^{-4}\left(4-\overline{h}/\overline{\sigma}\right)^{1.9474} & \text{if } 3.5<\left(\overline{h}/\overline{\sigma}\right)\le 4\\ 0 & \text{if } \left(\overline{h}/\overline{\sigma}\right)>4\end{cases} \quad (14)$$

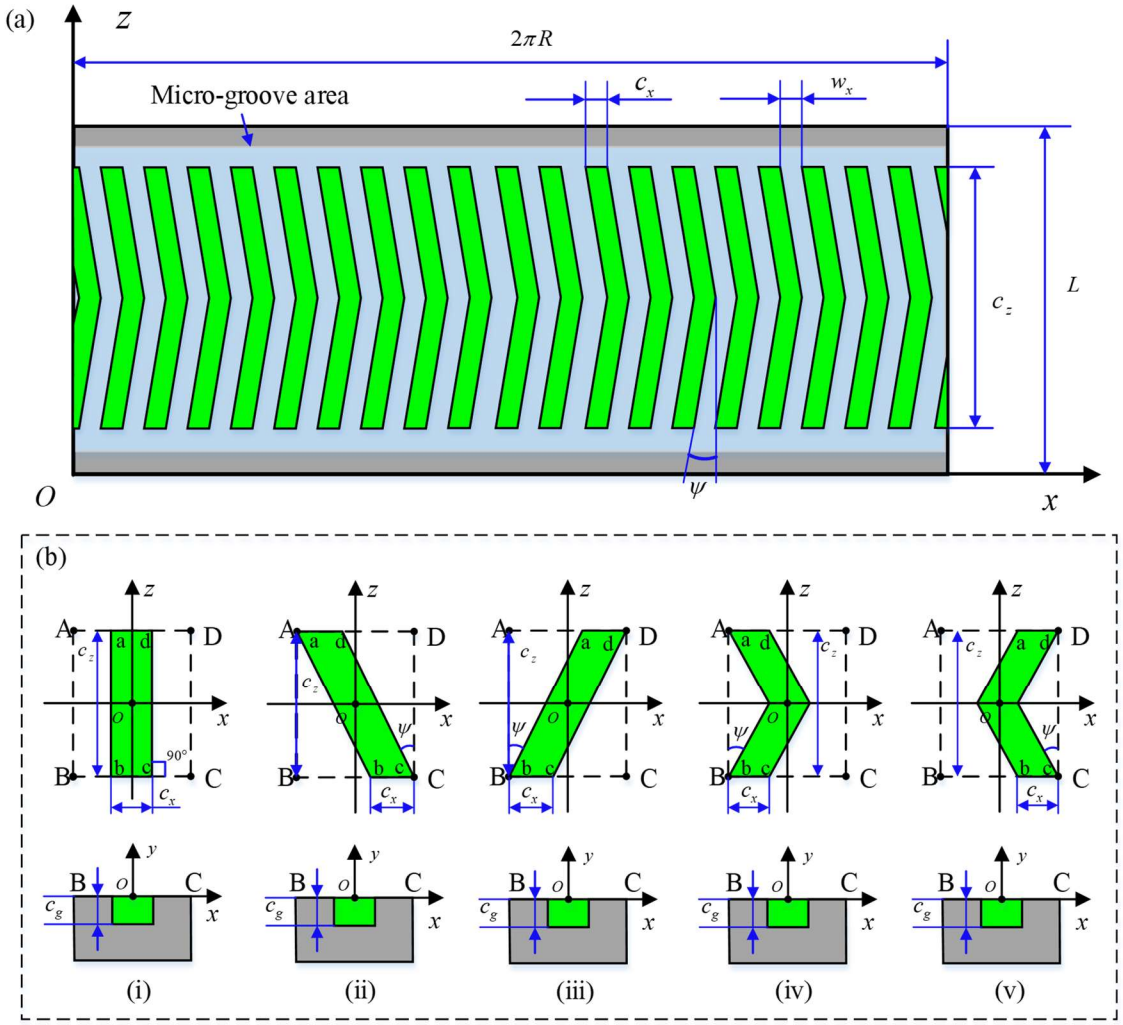

Figure 2. The schematic diagram of the expanded surface of micro-grooved bearing with different geometric shapes: (a) the expanded surface of micro-grooved bearing; (b) micro-grooves with different geometric shapes i.e., straight-groove, left spiral-groove, right spiral-groove, left herringbone-groove, right herringbone-groove.

2.3. Fluid film thickness

As shown in **Figure 1**, the fluid film thickness of journal bearing considering misalignment, elastic deformation and micro-groove is expressed as follows:

$$h=c+e\cos\left(\varphi-\theta\right)+e'\left(\frac{z}{L}-\frac{1}{2}\right)\cos\left(\varphi-\theta-\alpha\right)+\delta+h_g \quad (15)$$

where θ represents the attitude angle between the centre line and the y-axis, α represents misalignment angle between the attitude angle θ and $\overline{O_1O_2}$ line, δ represents the elastic

deformation of bearing shell, h_g represents the fluid film thickness in the micro-grooved region on the bearing surface.

To calculate the elastic deformation, Winkler hypothesis equation[45,46] is introduced as follows:

$$\delta = \frac{T_{\text{shell}}\left(1-\nu_0^2\right)}{E_b}\left(p + p_{asp}\right) \tag{16}$$

where T_{shell} represents the thickness of bearing shell, ν_0 is the equivalent Poisson's ratio related to the working conditions which is expressed as:

$$\upsilon_0 = \left(2\upsilon_b^2 / \left(1-\upsilon_b\right)\right)^{1/2} \tag{17}$$

Micro-grooves with different geometric shapes are displayed in **Figure 2**. The corresponding mathematical expressions of single micro-groove are expressed as follows:

- For non-micro-groove surface

$$h_g = 0; \text{ for non-groove region} \tag{18a}$$

- For straight-groove surface

$$h_g = \begin{cases} c_g, & \begin{cases} \left|x-x_o\right| \le \left(c_x/2\right) \\ \left|z-z_o\right| \le \left(c_z/2\right) \end{cases} \\ 0, & \text{for non-groove region} \end{cases} \tag{18b}$$

- For left spiral-groove surface

$$h_g = \begin{cases} c_g, & \begin{cases} \left|z-z_o\right| \le \left(c_z/2\right) \\ z-z_o \ge -\tan\psi\left(x-x_o\right) - \left(c_x/2\right)\tan(\pi/2-\psi) \\ z-z_o \le -\tan\psi\left(x-x_o\right) + \left(c_x/2\right)\tan(\pi/2-\psi) \end{cases} \\ 0, & \text{for non-groove region} \end{cases} \tag{18c}$$

- For right spiral-groove surface

$$h_g = \begin{cases} c_g, & \begin{cases} \left|z-z_o\right| \le \left(c_z/2\right) \\ z-z_o \ge \tan\psi\left(x-x_o\right) - \left(c_x/2\right)\tan(\pi/2-\psi) \\ z-z_o \le \tan\psi\left(x-x_o\right) + \left(c_x/2\right)\tan(\pi/2-\psi) \end{cases} \\ 0, & \text{for non-groove region} \end{cases} \tag{18d}$$

- For left herringbone-groove surface

$$h_g = \begin{cases} c_g, & \begin{cases} 0 \le z-z_o \le \left(c_z/2\right), & \begin{cases} z-z_o \ge -\tan\psi\left(x-x_o\right) - \left(c_x/2\right)\tan(\pi/2-\psi) \\ z-z_o \le -\tan\psi\left(x-x_o\right) + \left(c_x/2\right)\tan(\pi/2-\psi) \end{cases} \\ -\left(c_z/2\right) \le z-z_o < 0, & \begin{cases} z-z_o \ge \tan\psi\left(x-x_o\right) - \left(c_x/2\right)\tan(\pi/2-\psi) \\ z-z_o \le \tan\psi\left(x-x_o\right) + \left(c_x/2\right)\tan(\pi/2-\psi) \end{cases} \end{cases} \\ 0, & \text{for non-groove region} \end{cases} \tag{18e}$$

- For right herringbone-groove surface

$$h_g=\begin{cases} c_g, & \begin{cases} 0\le z-z_o\le (c_z/2), & \begin{cases} z-z_o\ge \tan\psi\,(x-x_o)-(c_x/2)\tan(\pi/2-\psi) \\ z-z_o\le \tan\psi\,(x-x_o)+(c_x/2)\tan(\pi/2-\psi) \end{cases} \\ -(c_z/2)\le z-z_o<0, & \begin{cases} z-z_o\ge -\tan\psi\,(x-x_o)-(c_x/2)\tan(\pi/2-\psi) \\ z-z_o\le -\tan\psi\,(x-x_o)+(c_x/2)\tan(\pi/2-\psi) \end{cases} \end{cases} \\ 0, \quad \text{for non-groove region} \end{cases} \tag{18f}$$

where c_x, c_z and c_g represent the length, width and depth of the micro-grooves in *x*, *z* and *y* directions, respectively, ψ represents the deflection angle between the side of the micro-groove and the *oz* axis. *ABCD* represents a single micro-groove calculation area, *abcd* represents a single micro-groove profile.

Substituting the dimensionless parameters of the equation (3) into equation (15), the dimensionless forms of fluid film thickness for bearing can be described as follows:

$$\overline{h}=1+\varepsilon\cos(\varphi-\theta)+\varepsilon'\left(Z-\frac{1}{2}\right)\cos(\varphi-\theta-\alpha)+\overline{h}_g+\overline{\delta} \tag{19}$$

where the misalignment eccentricity ratio ε' is expressed as follows:

$$\varepsilon'=D_m\varepsilon'_{\max} \tag{20}$$

where D_m is defined as the degree of misalignment which range are between 0 and 1. For an aligned journal bearing, $D_m=0$. $\varepsilon'_{\max}$ is defined as the maximum value of misalignment eccentricity ratio ε', and it is expressed as follows:[41]

$$\varepsilon'_{\max}=2\left(\left(1-\varepsilon^2\sin^2\alpha\right)^{1/2}-\varepsilon\left|\cos\alpha\right|\right) \tag{21}$$

2.4. The static and dynamic characteristics of journal bearing

2.4.1. The load carrying capacity and the attitude angle

The load carrying capacity denotes the external load that the journal bearing can support. The load carrying capacity includes hydrodynamic load and asperity contact load, whose components in the ξ and ζ directions are expressed as follows:[47]

$$\begin{aligned} W_\xi&=\int_0^L\int_0^{2\pi R}\left(p+p_{asp}\right)\sin(\varphi-\theta)\,dxdz=\left(\frac{\mu UR^2L}{c^2}\right)\left[\int_0^1\int_0^{2\pi}\left(\overline{p}+\overline{p}_{asp}\right)\sin(\varphi-\theta)\,d\varphi dZ\right] \\ W_\zeta&=-\int_0^L\int_0^{2\pi R}\left(p+p_{asp}\right)\cos(\varphi-\theta)\,dxdz=-\left(\frac{\mu UR^2L}{c^2}\right)\left[\int_0^1\int_0^{2\pi}\left(\overline{p}+\overline{p}_{asp}\right)\cos(\varphi-\theta)\,d\varphi dZ\right] \end{aligned} \tag{22}$$

The load carrying capacity and the attitude angle of journal bearing can be obtained as follows:

$$W=\sqrt{W_\xi^{\,2}+W_\zeta^{\,2}} \tag{23}$$

$$\theta=\tan^{-1}\left(W_\xi/W_\zeta\right) \tag{24}$$

It is worth mentioning that the components of the load carrying capacity of the $\xi\zeta$ coordinate system can be converted into o*xy* coordinate system by the formula, as following:

$$\begin{bmatrix} W_x & W_y \end{bmatrix}=\begin{bmatrix} W_\xi & W_\zeta \end{bmatrix}\begin{bmatrix} \cos\theta & \sin\theta \\ -\sin\theta & \cos\theta \end{bmatrix} \tag{25}$$

2.4.2. The frictional force and friction coefficient

The friction force is composed of hydrodynamic friction force due to lubricant shear and asperity contact friction force due to asperity peak shear.[43] The expression is as follows:

$$F = F_{vis} + F_{asp} \tag{26}$$

$$\begin{aligned} F_{vis} &= \int_0^L \int_0^{2\pi R} \left((1-\Theta)\frac{h}{2}\frac{\partial p}{\partial x}\phi_{fp} + (1-\Theta)\frac{\mu u}{h}\left(\phi_f + \phi_{fs}\right)\right) dxdz \\ &= \left(\frac{\mu URL}{c}\right)\left[\int_0^1 \int_0^{2\pi} \left((1-\Theta)\frac{\bar{h}}{2}\frac{\partial \bar{p}}{\partial x}\phi_{fp} + (1-\Theta)\frac{\bar{\mu}\bar{u}}{\bar{h}}\left(\phi_f + \phi_{fs}\right)\right) d\varphi dZ\right] \end{aligned} \tag{27}$$

$$F_{asp} = \int_0^L \int_0^{2\pi R} \left(\mu_{dry} p_{asp}\right) dxdz = \left(\frac{\mu URL}{c}\right)\left[\int_0^1 \int_0^{2\pi} \left(\bar{\mu}_{dry}\bar{p}_{asp}\right) d\varphi dZ\right] \tag{28}$$

where μ_{dry} represents the dry friction coefficient. ϕ_{fp}, ϕ_f, ϕ_{fs} represent the shear stress factors, whose values are determined as follows:

$$\phi_{fp} = 1 - De^{-s\left(\bar{h}/\bar{\sigma}\right)} \tag{29}$$

$$\phi_{fs} = \bar{V}_{rj}\Phi_{fs}\left(\bar{h}/\bar{\sigma}, \gamma_j\right) - \bar{V}_{rb}\Phi_{fs}\left(\bar{h}/\bar{\sigma}, \gamma_b\right) \tag{30a}$$

$$\Phi_{fs} = \begin{cases} A_3\left(h/\sigma\right)^{\alpha_4} e^{-\alpha_5(h/\sigma)+\alpha_6(h/\sigma)^2} & \text{if } 0.5 < \left(h/\sigma\right) < 7 \\ 0 & \text{if } \left(h/\sigma\right) \geq 7 \end{cases} \tag{30b}$$

$$\phi_f = \begin{cases} \frac{35}{32} z_f \left[\left(1-z_f{}^2\right)^3 \ln\left(300\left(z_f+1\right)\right) + z_{f1}\right] & \text{if } \left(\frac{\bar{h}}{\bar{\sigma}}\right) \leq 3 \\ \frac{35}{32} z_f \left[\left(1-z_f{}^2\right)^3 \ln\left(\frac{z_f+1}{z_f-1}\right) + z_{f2}\right] & \text{if } \left(\frac{\bar{h}}{\bar{\sigma}}\right) > 3 \end{cases} \tag{31}$$

$$z_f = \frac{\bar{h}}{3\bar{\sigma}}$$

$$\begin{aligned} z_{f1} &= \frac{1}{60}\left(-55 + 132z_f + 345z_f{}^2 - 160z_f{}^3 - 405z_f{}^4 + 60z_f{}^5 + 147z_f{}^6\right) \\ z_{f2} &= \frac{z_f}{15}\left(66 + 30z_f{}^4 - 80z_f{}^2\right) \end{aligned} \tag{32}$$

The determination of the constant values in equations (29) to (32) can be found in the literature[36]. Further, the friction coefficient can be calculated as follows:

$$f = \frac{F}{W} \tag{33}$$

2.4.3. The side leakage flow rate

The total side leakage flow rate is composed of two parts: the front side Q_{z1} and the rear side Q_{z2}, as follows:

$$\begin{aligned} Q_{z1} &= -\int_0^{2\pi R} \phi_z \frac{h^3}{12\mu}\frac{\partial p}{\partial z}\bigg|_{z=0} dx = -\left(\frac{cUR^2}{\mu L}\right)\int_0^{2\pi} \phi_z \frac{\bar{h}^3}{12}\frac{\partial \bar{p}}{\partial Z}\bigg|_{z=0} d\varphi \\ Q_{z2} &= -\int_0^{2\pi R} \phi_z \frac{h^3}{12\mu}\frac{\partial p}{\partial z}\bigg|_{z=L} dx = -\left(\frac{cUR^2}{\mu L}\right)\int_0^{2\pi} \phi_z \frac{\bar{h}^3}{12}\frac{\partial \bar{p}}{\partial Z}\bigg|_{z=1} d\varphi \end{aligned} \tag{34}$$

The total side leakage flow rate can be expressed as:

$$Q_z = \left|Q_{z1}\right| + \left|Q_{z2}\right| \tag{35}$$

2.4.4. The misaligned moment and direction angle

The misaligned moment of aligned journal bearing is absent, and those of misaligned journal bearing are expressed as follows:[47]

$$\begin{aligned} M_x &= \int_0^L \int_0^{2\pi R} \left(p + p_{asp}\right) R\left(z - \frac{L}{2}\right) \cos\varphi dx dz = \left(\frac{\mu U R^2 L^2}{c^2}\right)\left[\int_0^1 \int_0^{2\pi} \left(\overline{p} + \overline{p}_{asp}\right) \cos\varphi d\varphi dZ\right] \\ M_y &= \int_0^L \int_0^{2\pi R} \left(p + p_{asp}\right) R\left(z - \frac{L}{2}\right) \sin\varphi dx dz = \left(\frac{\mu U R^2 L^2}{c^2}\right)\left[\int_0^1 \int_0^{2\pi} \left(\overline{p} + \overline{p}_{asp}\right) \sin\varphi d\varphi dZ\right] \end{aligned} \tag{36}$$

The total misaligned moment and corresponding direction angle are expressed as follows:

$$M = \sqrt{M_x{}^2 + M_y{}^2} \tag{37}$$

$$\phi_M = \left(1 - \text{sign}M_y\right) \cdot 90^\circ + \text{sign}M_y \cdot \text{sign}M_x \cdot \arctan\left|M_x / M_y\right| \tag{38}$$

2.4.5. The stiffness and damping coefficients

With the mathematical perturbation method, a small displacement $\left(\Delta\overline{x}, \Delta\overline{y}\right)$ and velocity $\left(\Delta\dot{\overline{x}}, \Delta\dot{\overline{y}}\right)$ are generated at the equilibrium position of journal. The zeroth order and the first order Taylor expansions of the fluid film thickness and pressure represent steady and dynamic conditions. The dimensionless forms of the fluid film thickness and pressure with respect to small displacement and velocity are as follows:[48]

$$\overline{h} = \overline{h}_0 + \Delta\overline{h} = \overline{h}_0 + \Delta\overline{x}\sin\varphi + \Delta\overline{y}\cos\varphi \tag{39}$$

$$\overline{p} = \overline{p}_0 + \Delta\overline{p} = \overline{p}_0 + \overline{p}_x\Delta\overline{x} + \overline{p}_y\Delta\overline{y} + \overline{p}_{\dot{x}}\Delta\dot{\overline{x}} + \overline{p}_{\dot{y}}\Delta\dot{\overline{y}} \tag{40}$$

Substituting the perturbation equations of fluid film thickness (39) and fluid film pressure (40) into Reynolds equation (4), the dimensionless forms of the steady Reynolds and perturbation equations are obtained as follows:

$$\left[\frac{\partial}{\partial\varphi}\left(\phi_x\overline{h}^3\frac{\partial\overline{p}_\varsigma}{\partial\varphi}\right) + \frac{\partial}{\partial Z}\left(\phi_z\overline{h}^3\frac{\partial\overline{p}_\varsigma}{\partial Z}\right)\right]$$

$$= \begin{cases} 6\overline{u}\left(\phi_c\dfrac{\partial\left[\left(1-\Theta\right)\overline{h}_0\right]}{\partial\varphi} + \overline{\sigma}\dfrac{\partial\left[\left(1-\Theta\right)\phi_s\right]}{\partial\varphi}\right) & \left(\varsigma = 0\right) \\ -\dfrac{\partial}{\partial\varphi}\left(\phi_x 3\overline{h}_0^2\dfrac{\partial\overline{p}_0}{\partial\varphi}\sin\varphi\right) - \dfrac{\partial}{\partial Z}\left(\phi_z 3\overline{h}_0^2\dfrac{\partial\overline{p}_0}{\partial Z}\sin\varphi\right) + 6\overline{u}\cos\varphi & \left(\varsigma = x\right) \\ -\dfrac{\partial}{\partial\varphi}\left(\phi_x 3\overline{h}_0^2\dfrac{\partial\overline{p}_0}{\partial\varphi}\cos\varphi\right) - \dfrac{\partial}{\partial Z}\left(\phi_z 3\overline{h}_0^2\dfrac{\partial\overline{p}_0}{\partial Z}\cos\varphi\right) - 6\overline{u}\sin\varphi & \left(\varsigma = y\right) \\ 12\sin\varphi & \left(\varsigma = \dot{x}\right) \\ 12\cos\varphi & \left(\varsigma = \dot{y}\right) \end{cases} \tag{41}$$

where $\overline{h}_0$ represents the dimensionless fluid film thickness at the equilibrium position, $\overline{p}_0$, $\overline{p}_x$, $\overline{p}_y$, $\overline{p}_{\dot{x}}$, $\overline{p}_{\dot{y}}$ represent the dimensionless steady-state and perturbed pressures, respectively.

With the perturbation method, the hydrodynamic force can be calculated from the linear combination of the fluid film stiffness and damping coefficients as follows:

$$\begin{Bmatrix} W_x \\ W_y \end{Bmatrix} = \begin{Bmatrix} W_{x0} \\ W_{y0} \end{Bmatrix} + \begin{bmatrix} k_{xx} & k_{xy} \\ k_{yx} & k_{yy} \end{bmatrix} \begin{Bmatrix} \Delta\bar{x} \\ \Delta\bar{y} \end{Bmatrix} + \begin{bmatrix} c_{xx} & c_{xy} \\ c_{yx} & c_{yy} \end{bmatrix} \begin{Bmatrix} \Delta\dot{\bar{x}} \\ \Delta\dot{\bar{y}} \end{Bmatrix} \tag{42}$$

where W_x and W_y are the static hydrodynamic force in x and y directions at the equilibrium position of journal. Furthermore, after the steady-state and perturbed pressures are obtained, the fluid film stiffness and damping coefficients can then be calculated by the integration of perturbed pressures within the oil film land. The stiffness and damping coefficients of the fluid film can be expressed in matrix form as follows:[22,48]

$$\begin{bmatrix} k_{xx} & k_{xy} \\ k_{yx} & k_{yy} \end{bmatrix} = \begin{bmatrix} \left.\frac{\partial W_x}{\partial x}\right|_0 & \left.\frac{\partial W_x}{\partial y}\right|_0 \\ \left.\frac{\partial W_y}{\partial x}\right|_0 & \left.\frac{\partial W_y}{\partial y}\right|_0 \end{bmatrix} = \left(\frac{\mu U R^2 L}{c^3}\right) \begin{bmatrix} \int_0^1\int_0^{2\pi} \bar{p}_x \sin\varphi d\varphi dZ & \int_0^1\int_0^{2\pi} \bar{p}_y \sin\varphi d\varphi dZ \\ \int_0^1\int_0^{2\pi} \bar{p}_x \cos\varphi d\varphi dZ & \int_0^1\int_0^{2\pi} \bar{p}_y \cos\varphi d\varphi dZ \end{bmatrix} \tag{43}$$

$$\begin{bmatrix} c_{xx} & c_{xy} \\ c_{yx} & c_{yy} \end{bmatrix} = \begin{bmatrix} \left.\frac{\partial W_x}{\partial \dot{x}}\right|_0 & \left.\frac{\partial W_x}{\partial \dot{y}}\right|_0 \\ \left.\frac{\partial W_y}{\partial \dot{x}}\right|_0 & \left.\frac{\partial W_y}{\partial \dot{y}}\right|_0 \end{bmatrix} = \left(\frac{\mu U R^2 L}{c^3 \omega}\right) \begin{bmatrix} \int_0^1\int_0^{2\pi} \bar{p}_{\dot{x}} \sin\varphi d\varphi dZ & \int_0^1\int_0^{2\pi} \bar{p}_{\dot{y}} \sin\varphi d\varphi dZ \\ \int_0^1\int_0^{2\pi} \bar{p}_{\dot{x}} \cos\varphi d\varphi dZ & \int_0^1\int_0^{2\pi} \bar{p}_{\dot{y}} \cos\varphi d\varphi dZ \end{bmatrix} \tag{44}$$

3. Solution procedure

The effects of misalignment and micro-groove parameters on the lubrication performance of journal bearings with consideration of surface roughness and elastic deformation are numerically analyzed. Simulation has been carried out by solving the average Reynolds equation with mass conservation and the fluid film thickness equations includes multiple factors. As shown in **Figure 3**, the solution procedure is given as follows:

Step 1: Input operating conditions, initialize mesh parameters.
Step 2: Assume the initial fluid film thickness that determines whether surface roughness, degree of misalignment, micro-groove depth and elastic deformation should be considered.
Step 3: Solve the Reynolds equation (4) using the finite difference method to obtain the hydrodynamic pressure, and solve the asperity contact equation (12) to obtain the contact pressure.
Step 4: Solve the elastic deformation equation (16) to obtain the elastic deformation.
Step 5: Check whether the solutions are converged according to the criterions (45). If satisfied, continue to the next step, if not, the fluid film thickness needs to be recalculated and updated, and return to step 2.
Step 6: Calculate the components of the load carrying capacity, check whether the attitude angle is converged according to the criterion (46). If satisfied, continue to the next step, if not, adjust the attitude angle, return to step 2.
Step 7: Solve the perturbated Reynolds equations (41) using the finite difference method to obtain the perturbed pressures.
Step 8: Check whether the solutions are converged according to the criterions (45). If satisfied, continue to the next step, if not, adjust the perturbation pressures, return to step 5.
Step 9: Finally, calculate the static and dynamic performance parameters of journal bearing.

$$\frac{\sum_{i=1}^{m+1}\sum_{j=1}^{n+1}\left|\bar{p}(i,j)_\varsigma^{(new)} - \bar{p}(i,j)_\varsigma^{(old)}\right|}{\sum_{i=1}^{m+1}\sum_{j=1}^{n+1}\left|\bar{p}(i,j)_\varsigma^{(old)}\right|} \le 1.0\times10^{-6}, \quad \frac{\sum_{i=1}^{m+1}\sum_{j=1}^{n+1}\left|\Theta(i,j)_\varsigma^{(new)} - \Theta(i,j)_\varsigma^{(old)}\right|}{\sum_{i=1}^{m+1}\sum_{j=1}^{n+1}\left|\Theta(i,j)_\varsigma^{(new)}\right|} \le 1.0\times10^{-6} \tag{45}$$

$$\left|\frac{W_x}{W_y}\right| \le 1.0\times10^{-4} \tag{46}$$

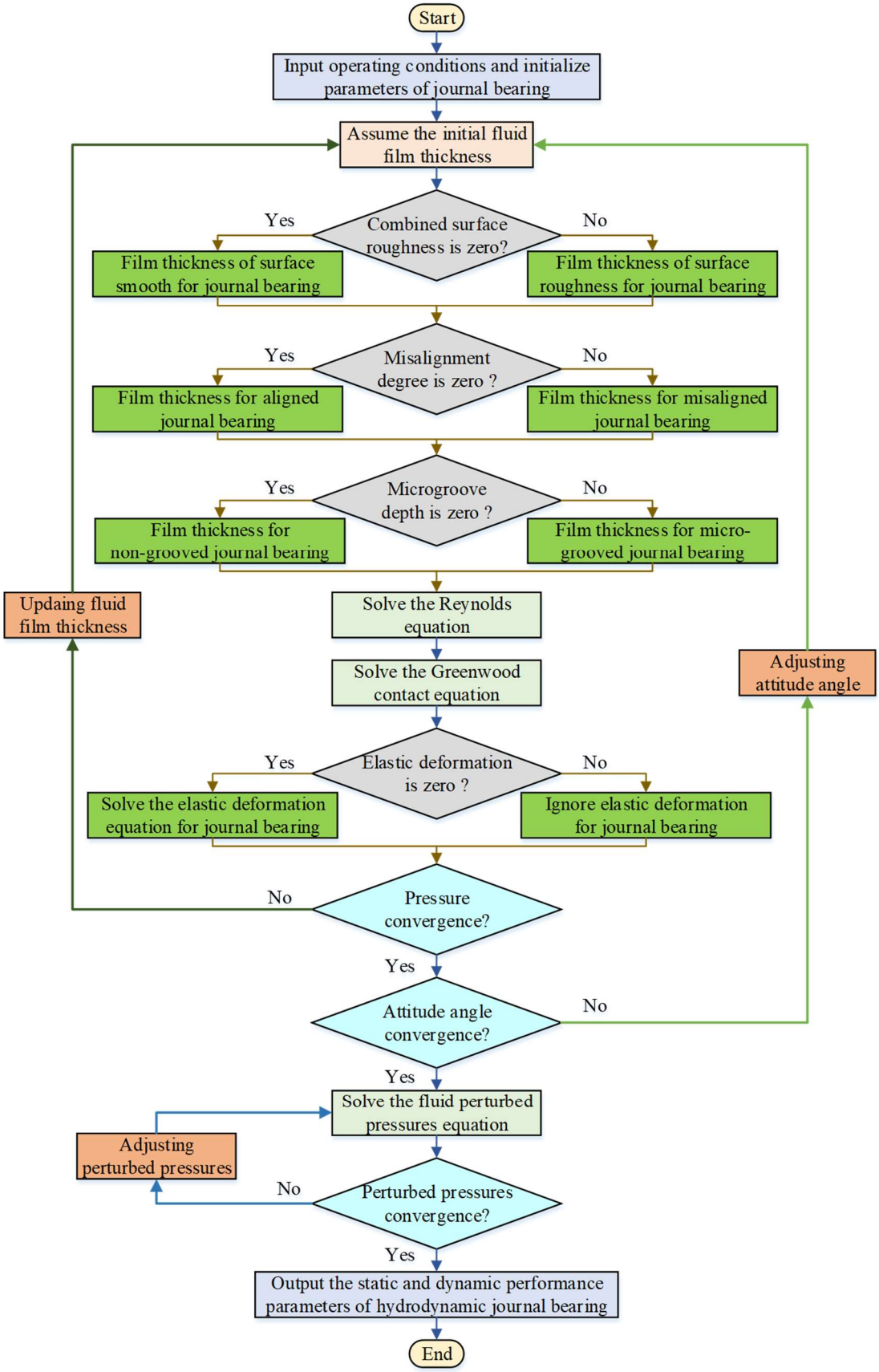

Figure 3. The flowchart of the global numerical solution procedure.

4. Results and discussion

As shown in **Figure** 4, micro-grooves with different geometric shapes i.e., straight-groove, left spiral-groove, right spiral-groove, left herringbone-groove and right herringbone-groove are investigated. To numerically analyzed the effects of the eccentricity ratio, degree of misalignment, misalignment angle, micro-groove deflection angle and depth on the lubrication performance of journal bearings. Furthermore, local distribution of textures can generate additional hydrodynamic lift compared to full distribution of textures.[30,49] Therefore, the distributions of five micro-grooves are assumed to be located within the convergent wedge where the bearing performance can be significantly improved in the following analysis. **Table 1** lists simulation parameters for geometrical parameters of the bearing and micro-groove as well as the operating condition.

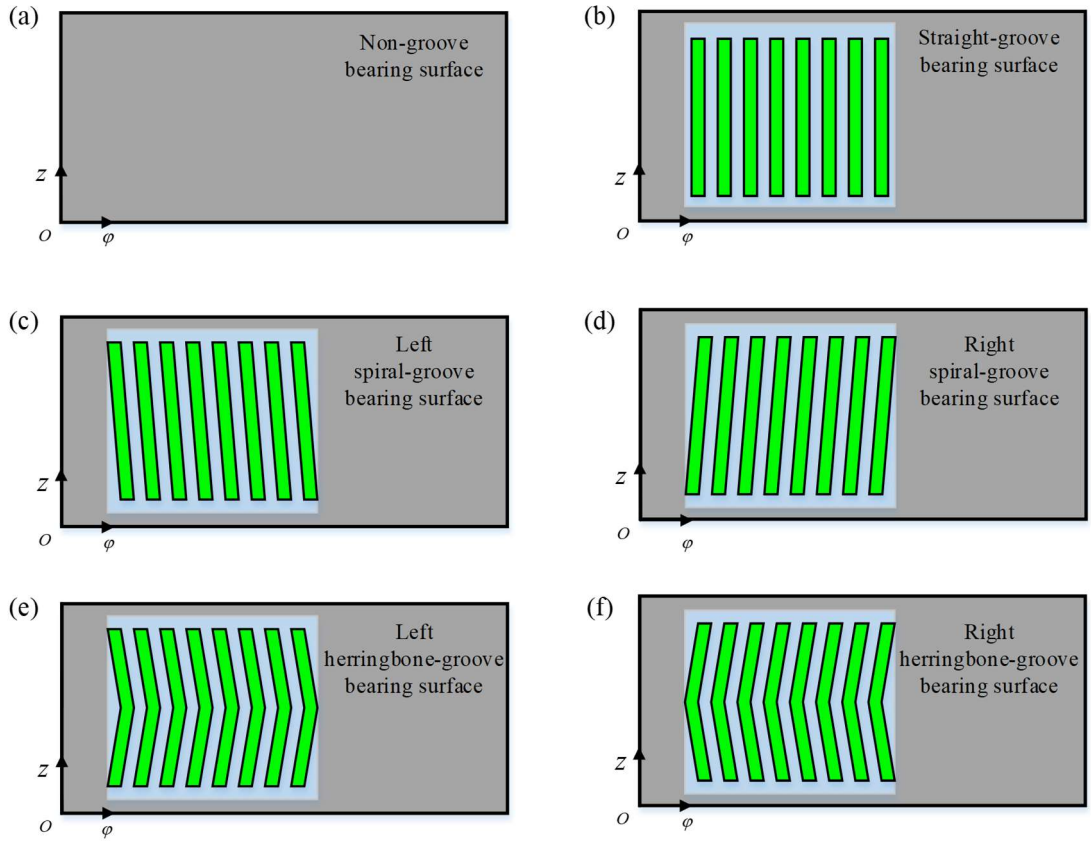

Figure 4. Micro-groove distribution with different geometric shapes i.e., straight-groove, left spiral-groove, right spiral-groove, left herringbone-groove, right herringbone-groove.

Table 1. Simulation parameters.

Parameters	Value	Parameters	Value
Bearing radius, R	50 mm	Dry friction coefficient, μ_{dry}	0.1
Bearing length, L	100 mm	combined surface roughness, σ	0.5 μm
Radial clearance, c	0.1 mm	the curvature radius of asperities, β	2 μm
Eccentricity ratio, ε	0.5	the density of asperities, η	0.5 μm^{-2}
Rotation speed, ω	2000 rpm	Surface orientation, γ	1
Lubricant viscosity, μ	0.01 Pa·s	Mic-groove length, c_x	10 mm
Bearing shell thickness, T_{shell}	1.5 mm	Mic-groove width, c_z	60 mm
Elastic modulus of bearing, E_b	65 GPa	Mic-groove depth, c_g	20 μm
Elastic modulus of journal, E_j	210 GPa	Mic-groove angle, ψ	60°
Poisson ratio of bearing, υ_b	0.3	Mic-groove number, N_g	8
Poisson ratio of journal, υ_j	0.3	Circumferential groove region	50°-194°

Degree of misalignment, D_m	0.5	Circumferential groove ratio, Λ_φ	0.4
Angle of misalignment, α	0°	Axial groove ratio, Λ_L	0.6

4.1. Model validation

In this section, in order to verify the accuracy of the developed model, the present results are compared with those of the published literature. The calculated results are first verified for the journal alignment and misalignment by comparing with the results of Jang and Khonsari[41], whose bearing parameters are listed in **Table 2**. **Table 3** lists the comparison results of static characteristic parameters between the present and Jang and Khonsari[41]. It can be observed from the data listed in the table that the obtained values match well with reference values. In order to better demonstrate the differences for misalignment and alignment of journal, the 3D distributions of fluid film thickness, pressure and cavitation fraction are given in **Figure 5**. Next, as shown in **Table 4**, the present numerical results of the dynamic characteristic parameters are compared with the results of Zhang et al.[50] and the results of Xie et al.[22] for journal bearing at eccentricity ratios of 0.2, 0.4 and 0.8. The bearing parameters are 2×150° circular bearing with a width-diameter ratio of 1.2. The dynamic characteristic parameters are unified into the same dimensionless form. Small differences exist between the present results and reference. Finally, in order to further verify the developed elastohydrodynamic lubrication model of micro-grooved bearing, the comparison between the experimental and numerical results of Gong et al.[30] with the numerical results of the present is given in **Figure 6**. The simulation/test parameters of Gong et al.[30] on water-lubricated bearings with microgroove are listed in **Table 5**. The approximately overlapping results verify the accuracy of this model.

Table 2. Bearing parameters by Jang and Khonsari[41].

Parameters	Value
Journal radius	20 mm
Bearing width	80 mm
Radial clearance	30 μm
Rotation speed	2500 rpm
Lubricant viscosity	0.02 Pa·s

Table 3. Comparison of static characteristic parameters of aligned/misaligned journal bearings.

	Results of the present		Results of Jang and Khonsari[41]	
Eccentricity ratio, ε	0.392	0.378	0.392	0.378
Degree of misalignment, D_m	0	0.53	0	0.53
Angle of misalignment, $\alpha\left(^\circ\right)$	–	121	–	121
Maximum pressure, $P_{\max}\left(\mathrm{MPa}\right)$	5.82	7.02	5.90	6.81
Load carrying capacity, $W\left(\mathrm{N}\right)$	19866.35	19975.53	20000	20000
Attitude angle, $\theta\left(^\circ\right)$	67.75	65.26	69.1	68.0
Friction coefficient, f	0.0039	0.0040	0.0039	0.0040
Side leakage flow rate, $Q_z\left(\mathrm{cm^3/s}\right)$	2.75	2.89	2.9	3.1
Moment, $M\left(\mathrm{N\,m}\right)$	–	79.52	–	76
Moment direction angle, $\phi_M\left(^\circ\right)$	–	246.43	–	224.5

Table 4. Comparison of dynamic characteristic parameters of journal bearings.

Results	ε	K_{xx}	K_{xy}	K_{yx}	K_{yy}	C_{xx}	C_{xy}	C_{yx}	C_{yy}
Zhang et al.[49]	0.2	0.6758	-0.6652	2.994	0.8587	1.405	0.7352	0.7352	6.090
Xie et al.[21]	0.2	0.6748	-0.6640	3.005	0.8570	1.414	0.7230	0.7220	6.125
the present	0.2	0.6770	-0.6661	3.006	0.8593	1.413	0.7361	0.7363	6.131

Zhang et al.[49]	0.4	1.788	-1.050	4.799	2.438	2.565	2.215	2.215	10.110
Xie et al.[21]	0.4	1.787	-1.048	4.810	2.437	2.556	2.217	2.215	10.149
the present	0.4	1.791	-1.061	4.818	2.442	2.571	2.221	2.219	10.132
Zhang et al.[49]	0.8	9.634	2.466	26.320	43.230	6.196	10.500	10.500	53.730
Xie et al.[21]	0.8	11.000	2.563	28.766	41.828	7.326	10.554	10.568	57.797
the present	0.8	10.859	2.543	27.956	44.112	7.225	10.856	10.605	55.336

Table 5. Simulation/test parameters of water-lubricated bearings with microgroove.

Parameters	Value	Parameters	Value
Shaft radius	30 mm	Bearing material	Thordon
Inner radius of lining	30.13 mm	Shaft material	Aluminum alloy
Outer radius of lining	37.63 mm	Bearing angle	60°
Block length	100 mm	Micro-groove width	0.4 mm
Rotational speed	1400 rpm	Micro-groove depth	50 μm
Eccentricity ratio	0.679	Bridge width	1.6 mm

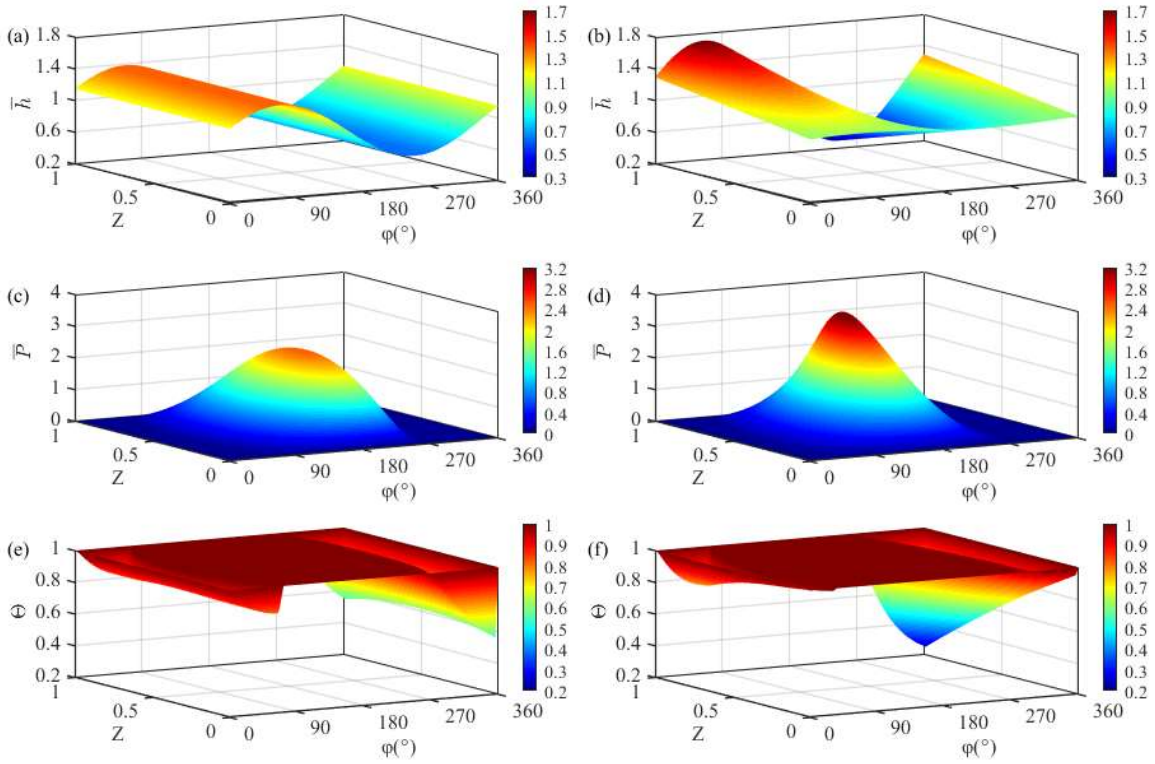

Figure 5. Dimensionless distributions of fluid film thickness, pressure and cavitation fraction for journal bearings: (a), (c) and (e) three dimensionless distributions for aligned journal bearings; (b), (d) and (f) three dimensionless distributions for misaligned journal bearings.

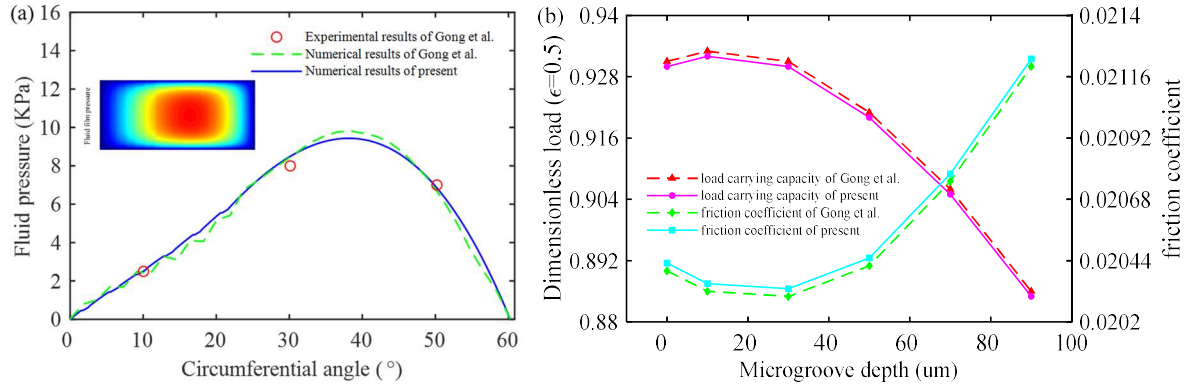

Figure 6. Model validation of lubrication performance for micro-grooved journal bearings: (a) circumferential distribution of fluid film pressure; (b) load carrying capacity and friction coefficient as the function of micro-groove depth.

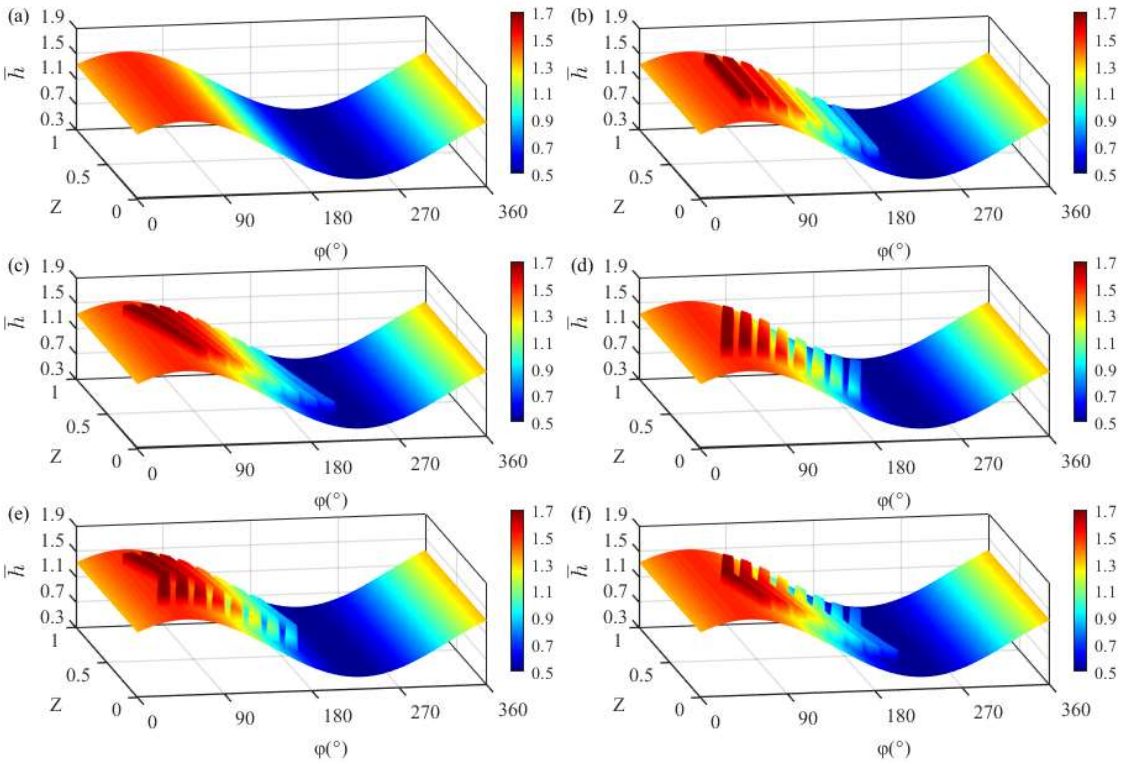

Figure 7. The comparisons of micro-grooves with different geometric shapes on fluid film thickness distribution of aligned journal bearings: (a) non-groove; (b) straight-groove; (c) left spiral-groove; (d) right spiral-groove; (e) left herringbone-groove; (f) right herringbone-groove.

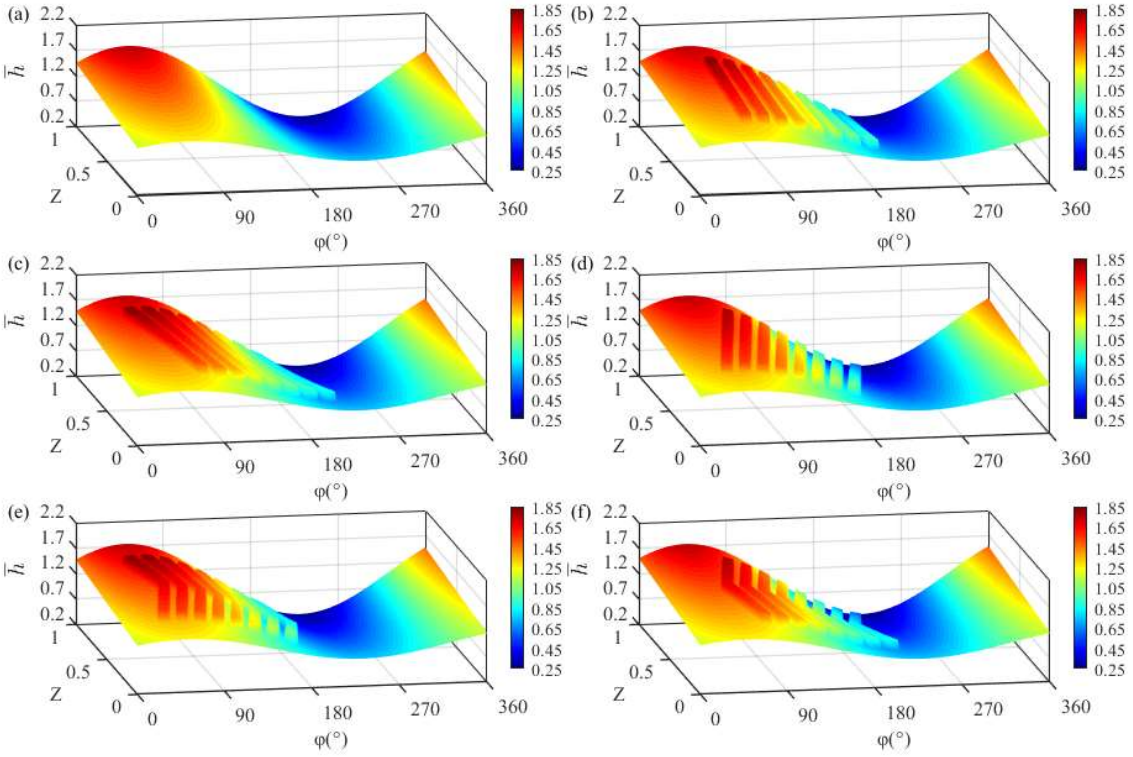

Figure 8. The comparisons of micro-grooves with different geometric shapes on fluid film thickness distribution of misaligned journal bearings: (a) non-groove; (b) straight-groove; (c) left spiral-groove; (d) right spiral-groove; (e) left herringbone-groove; (f) right herringbone-groove.

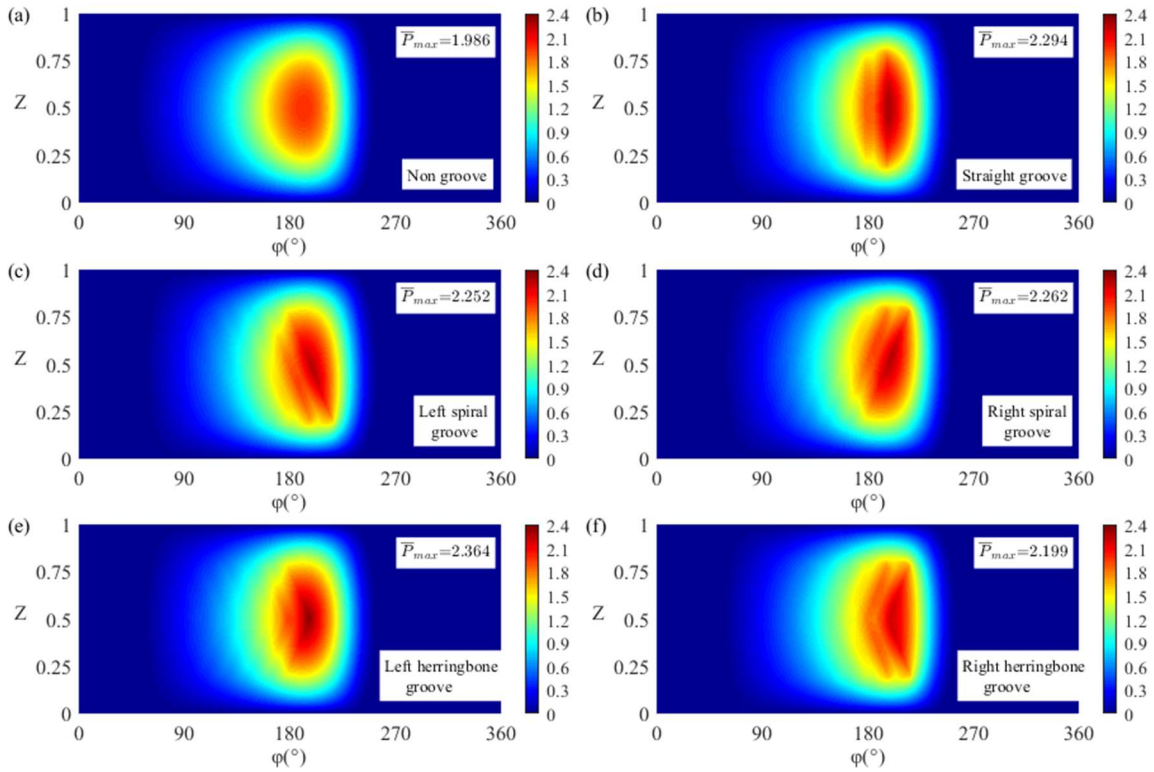

Figure 9. The comparisons of micro-grooves with different geometric shapes on fluid pressure distribution of aligned journal bearings: (a) non-groove; (b) straight-groove; (c) left spiral-groove; (d) right spiral-groove; (e) left herringbone-groove; (f) right herringbone-groove.

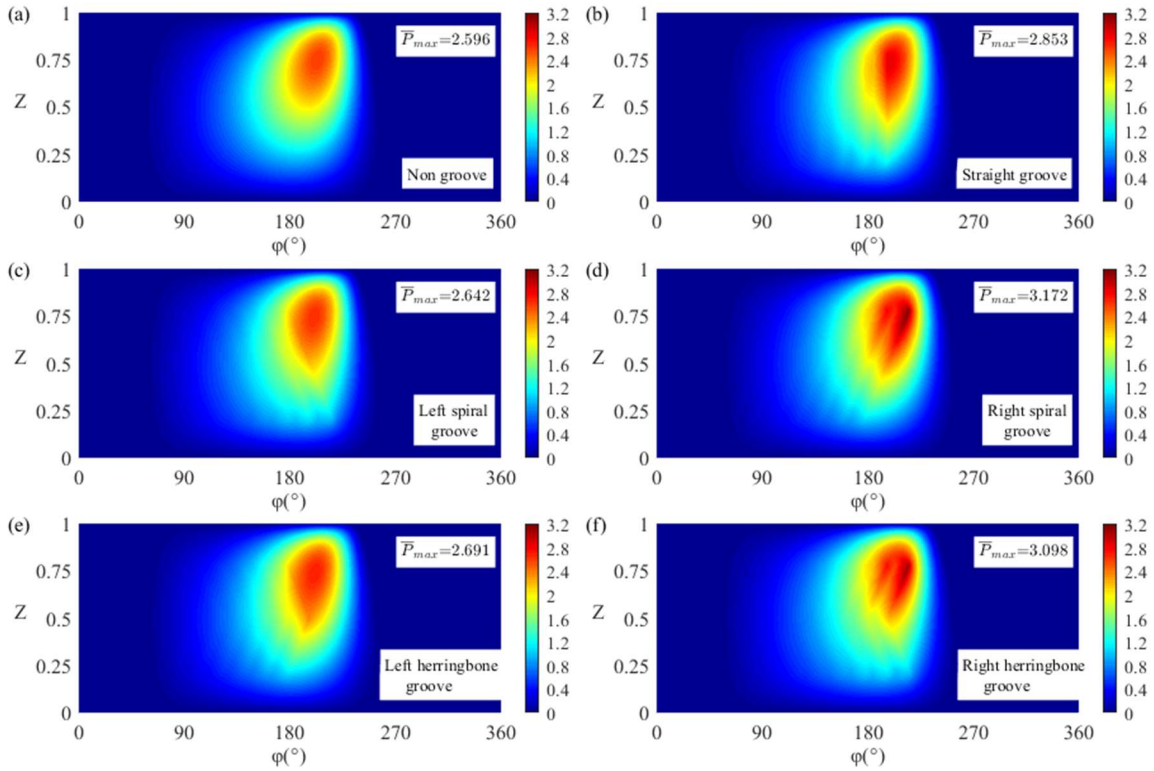

Figure 10. The comparisons of micro-grooves with different geometric shapes on fluid pressure distribution of misaligned journal bearings: (a) non-groove; (b) straight-groove; (c) left spiral-groove; (d) right spiral-groove; (e) left herringbone-groove; (f) right herringbone-groove.

4.2. Fluid film thickness and pressure distributions

In this section, the effects of micro-grooves with different geometric shapes on the fluid film thickness and pressure distributions of aligned and misaligned journal bearings are analyzed. As shown in **Figure 7** and **8**, the minimum film thickness of aligned journal bearings occurs around φ =229.8°, whereas the minimum film thickness of misaligned journal bearings occurs around φ =233.5°. It is clear that misalignment causes the deflection of fluid film thickness and decreases the minimum fluid film thickness.

The corresponding pressure distributions are then calculated and displayed in **Figure 9** and **10**. It can be observed that the journal misalignment mainly affects the film pressure distribution in the axial direction and the location where the pressure peaks appear. For the aligned journal bearing, the maximum fluid film pressures of straight-groove, left spiral-groove, right spiral-groove, left herringbone-groove, and right herringbone-groove are increased by 15.51%, 13.39%, 13.90%, 19.03%, and 10.73%, respectively, compared with that of no-groove. For the misaligned journal bearing, the maximum fluid film pressures of straight-groove, left spiral-groove, right spiral-groove, left herringbone-groove, and right herringbone-groove are increased by 9.90%, 1.77 %, 22.19%, 3.66%, and 19.34%, respectively, compared with that of no-groove. Whether or not journal misalignment is considered, the presence of micro-grooves on the bearing surface increases the maximum fluid film pressure due to additional hydrodynamic effect is generated. In addition, the amount of increase in the maximum fluid film pressure depends on the geometric shape of the micro-groove.

4.3. Effect of the eccentricity ratio

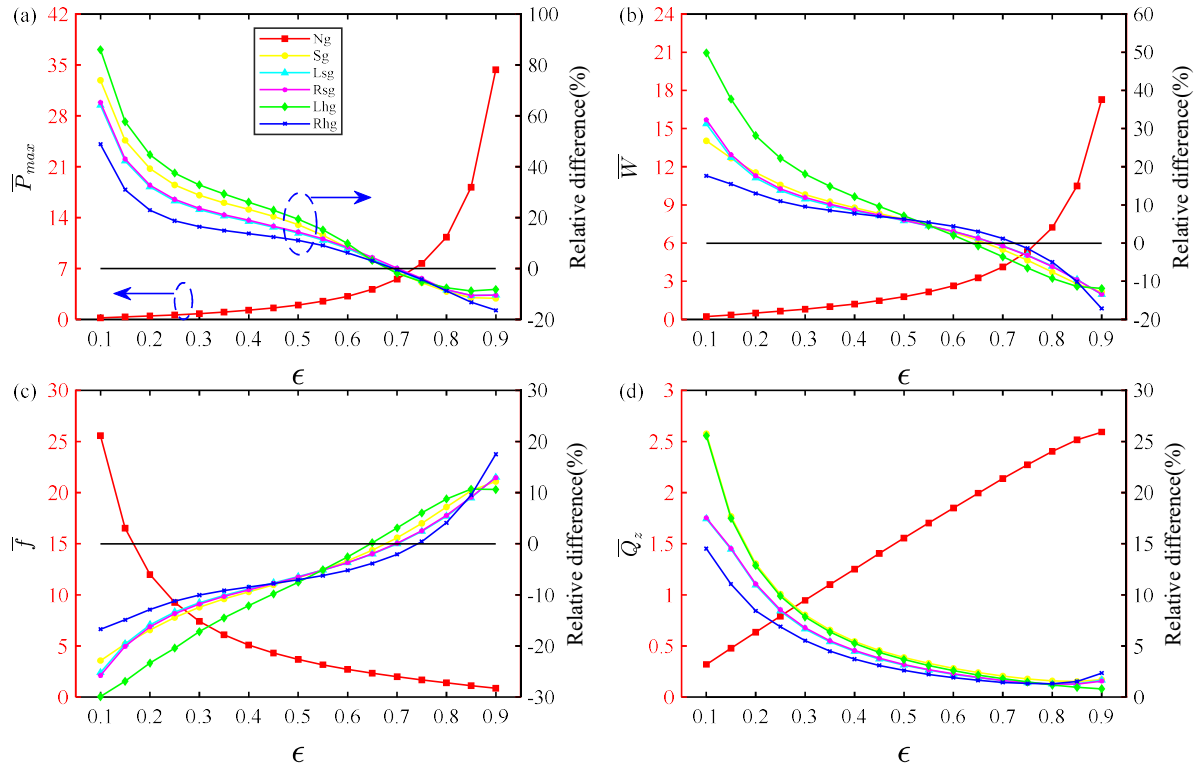

Figure 11. The effect of eccentricity ratio on the dimensionless static performance parameters of aligned journal bearings under micro-grooves with different geometric shapes: (a) the maximum fluid pressure; (b) the load carrying capacity; (c) the friction coefficient; (d) the side leakage flow rate.

In this section, the effects of the eccentricity ratio on the lubrication performance of aligned and misaligned micro-grooved journal bearings are analyzed. The static characteristic

parameters are displayed in **Figure 11** and **12**, while the dynamic characteristic parameters are displayed in **Figure 13** and **14**. The eccentricity ratio ranges from 0.1 to 0.9.

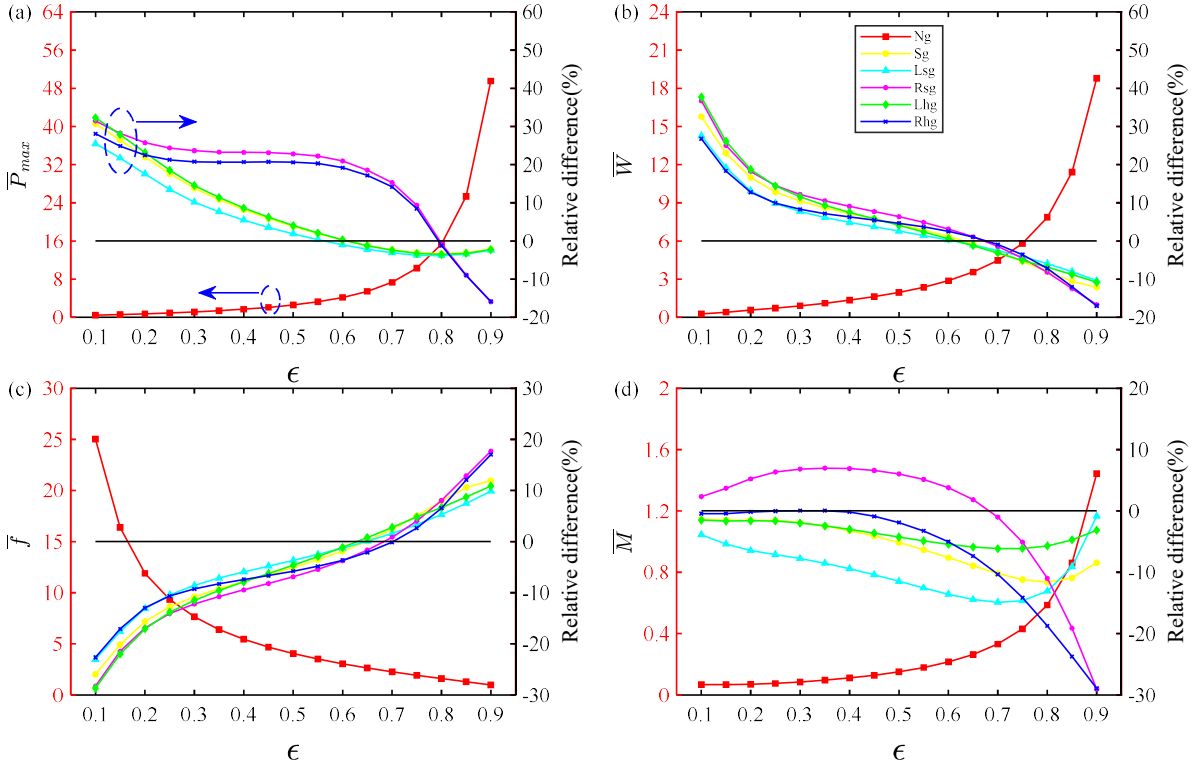

Figure 12. The effects of eccentricity ratio on the dimensionless static performance parameters of misaligned journal bearings under micro-grooves with different geometric shapes: (a) the maximum fluid pressure; (b) the load carrying capacity; (c) the friction coefficient; (d) the total misaligned moment.

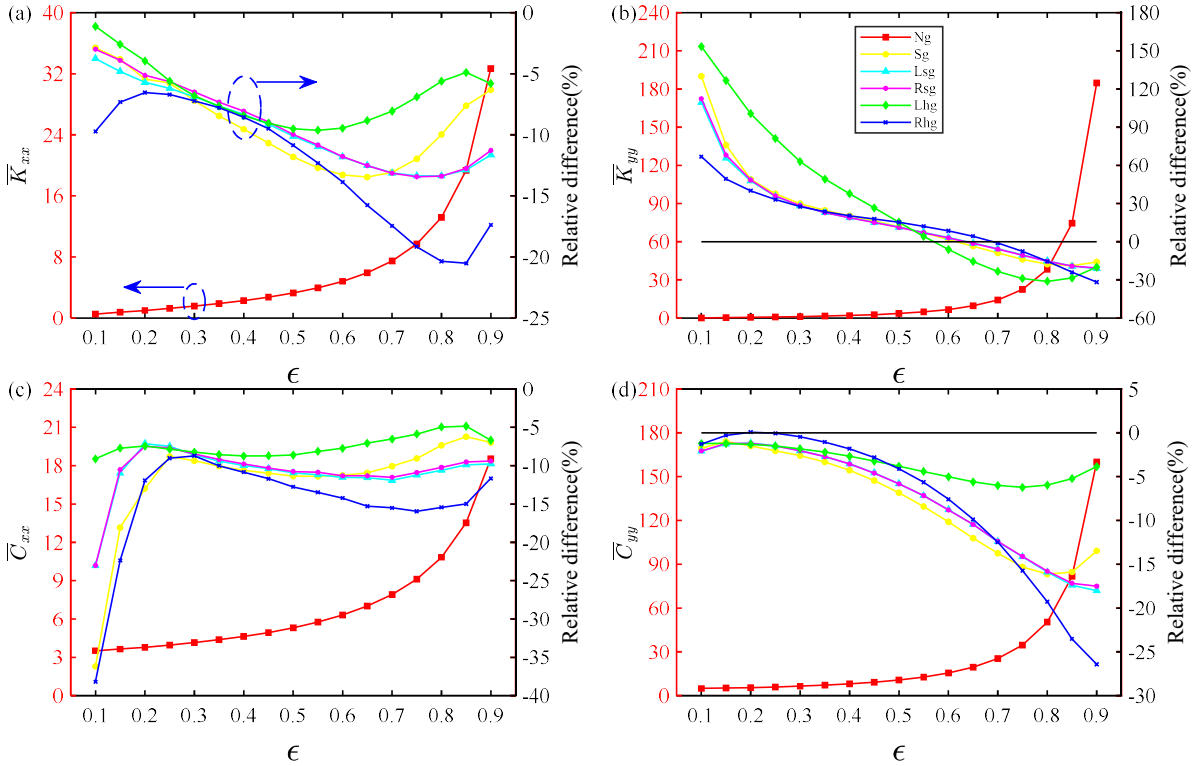

Figure 13. The effects of eccentricity ratio on the dimensionless dynamic performance parameters of aligned journal bearings under micro-grooves with different geometric shapes: (a) and (b) the main stiffness coefficients; (c) and (d) the main damping coefficients.

As the eccentricity ratio increases, as shown in **Figure 11** and **12**, the maximum fluid film pressure, the load carrying capacity and the misaligned moment increases especially for eccentricity ratio larger than 0.3 because the hydrodynamic effect is unobvious at small eccentricity ratio. An opposite trend is observed for the friction coefficient. The side leakage flow rate increases approximately linearly. Furthermore, under fixed eccentricity ratio, the maximum fluid film pressure of the misaligned journal bearings is larger than those of the aligned journal bearings due to the stronger hydrodynamic effect induced by the journal misalignment. Under the chosen value of the eccentricity ratio is 0.3, for the aligned journal bearing, the friction coefficients of straight-groove, left spiral-groove, right spiral-groove, left herringbone-groove, and right herringbone-groove are decreased by 12.41%, 11.52%, 11.80%, 17.19%, and 10.03%, respectively, compared with that of no-grooved journal bearing; for the misaligned journal bearing, the friction coefficients of straight-groove, left spiral-groove, right spiral-groove, left herringbone-groove, and right herringbone-groove are decreased by 10.79%, 8.59%, 12.22%, 11.49%, and 9.27%, respectively, compared with that of no-grooved journal bearing. The friction coefficient is used as an important index to evaluate the friction reduction effect of micro-grooved surface.

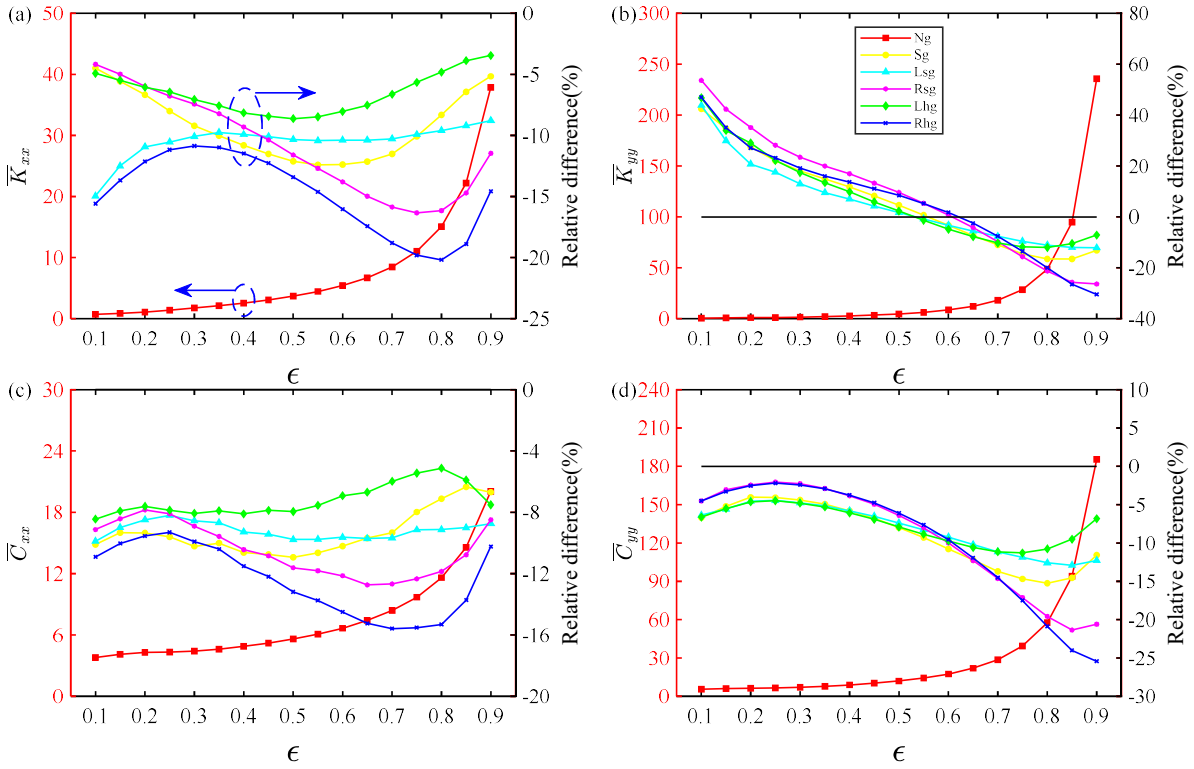

Figure 14. The effects of eccentricity ratio on the dimensionless dynamic performance parameters of misaligned journal bearings under micro-grooves with different geometric shapes: (a) and (b) the main stiffness coefficients; (c) and (d) the main damping coefficients.

As the eccentricity ratio increases, as shown in **Figure 13** and **14**, the main stiffness coefficients and the main damping coefficients increase especially for eccentricity ratio larger than 0.3. Except that the K_{yy} of micro-grooves are greater than that of non-groove at a smaller eccentricity ratio, the other values of dynamic characteristics are smaller than that of non-groove. The direct stiffness coefficient K_{yy} significantly changes due to the external load acts in the y direction, thence, the direct stiffness coefficient K_{yy} is mainly analyzed as an index for the improvement of the dynamic characteristic of micro-grooved bearing.[50] Under the chosen value of the eccentricity ratio is 0.3, for the aligned journal bearing, the direct stiffness coefficients K_{yy} of straight-groove, left spiral-groove, right spiral-groove, left herringbone-groove, and right herringbone-groove are increased by 29.99%, 28.10%,

28.42%, 63.01%, and 27.63%, respectively, compared with that of no-grooved journal bearing; for the misaligned journal bearing, the direct stiffness coefficients K_{yy} of straight-groove, left spiral-groove, right spiral-groove, left herringbone-groove, and right herringbone-groove are increased by 18.06%, 12.98%, 23.43%, 17.42%, and 19.17%, respectively, compared with that of no-grooved journal bearing.

It is observed that the static and dynamic characteristics of journal bearings with micro-grooves exhibits an obvious improvement at relatively small eccentricity ratio, but this improvement weakens at a large eccentricity ratio from the relative difference curve. It can be found that the degree of improvement in lubrication performance of journal bearings depend on the geometrical shapes of micro-groove. The optimal micro-groove geometric shape is different for aligned and misaligned journal bearings due to the change of the fluid film pressure distribution induced by the journal misalignment. The deflection direction of right spiral-groove is consistent with the inclination direction of the fluid pressure distribution, thus making the optimal micro-groove geometric shape of misaligned journal bearings different from that of aligned journal bearings.

4.4. Effect of the misalignment

In this section, the effects of the degree of misalignment and misalignment angle on the lubrication performance of micro-grooved journal bearings are analyzed. The eccentricity ratio is assumed as 0.5. The degree of misalignment ranges from 0 to 0.9. D_m closing to 0 indicates an aligned journal, while D_m closing to 1 indicates a maximum misaligned journal. The variation of the misalignment angle ranging from 0° to 180° is studied.

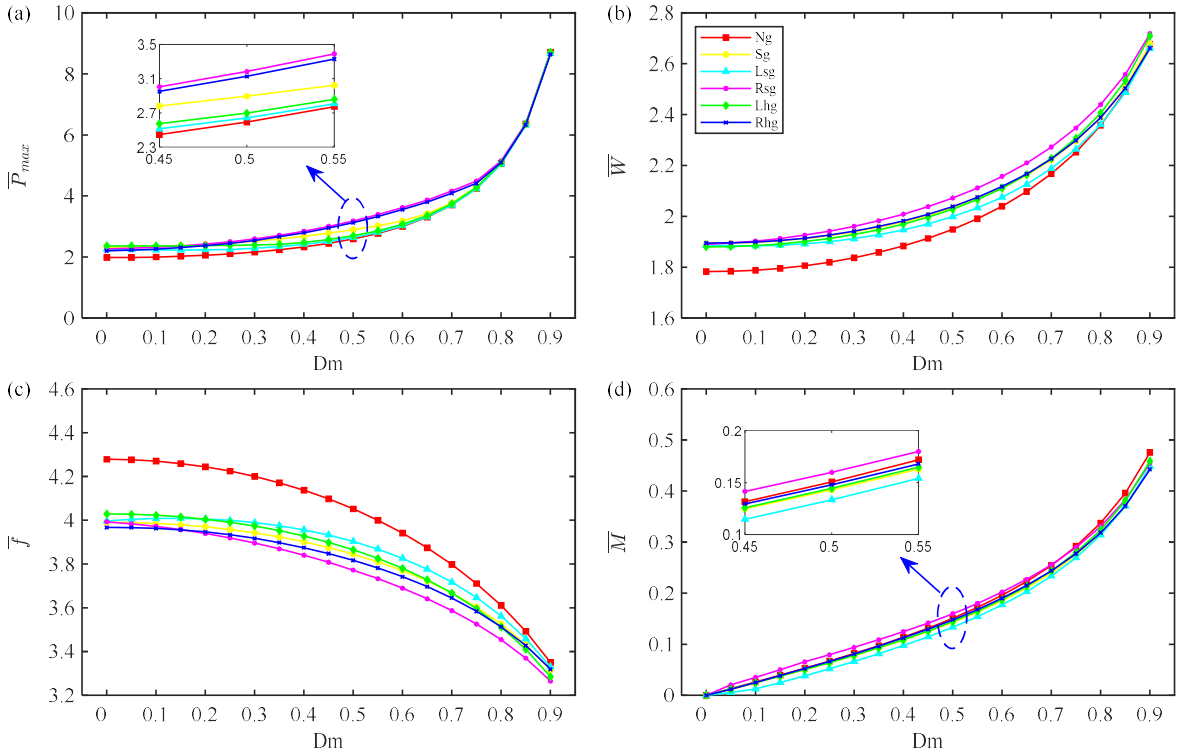

Figure 15. The effects of degree of misalignment on the dimensionless static performance parameters of misaligned journal bearings under micro-grooves with different geometric shapes: (a) the maximum fluid pressure; (b) the load carrying capacity; (c) the friction coefficient; (d) the total misaligned moment.

4.4.1. Effect of the degree of misalignment

Figure 15 and 16 show the static and dynamic characteristic parameters of micro-grooved journal bearings with different degrees of misalignment. As shown in **Figure 15**, with the degree of misalignment increases, the maximum fluid film pressure and the load carrying

capacity first increase slowly and then sharply, the friction coefficient first decreases slowly and then sharply, the misaligned moment gradually increase due to the larger pressure gradient. As the degree of misalignment increases, the minimum fluid film thickness decreases that result in a stronger hydrodynamic effect due to the convergence ratio in the axial direction increases with degree of misalignment. Under the chosen value of the degree of misalignment is 0.5, the friction coefficients of straight-groove, left spiral-groove, right spiral-groove, left herringbone-groove, and right herringbone-groove are decreased by 5.09%, 3.66%, 6.90%, 4.61%, and 5.80%, respectively, compared with that of no-grooved misaligned journal bearing.

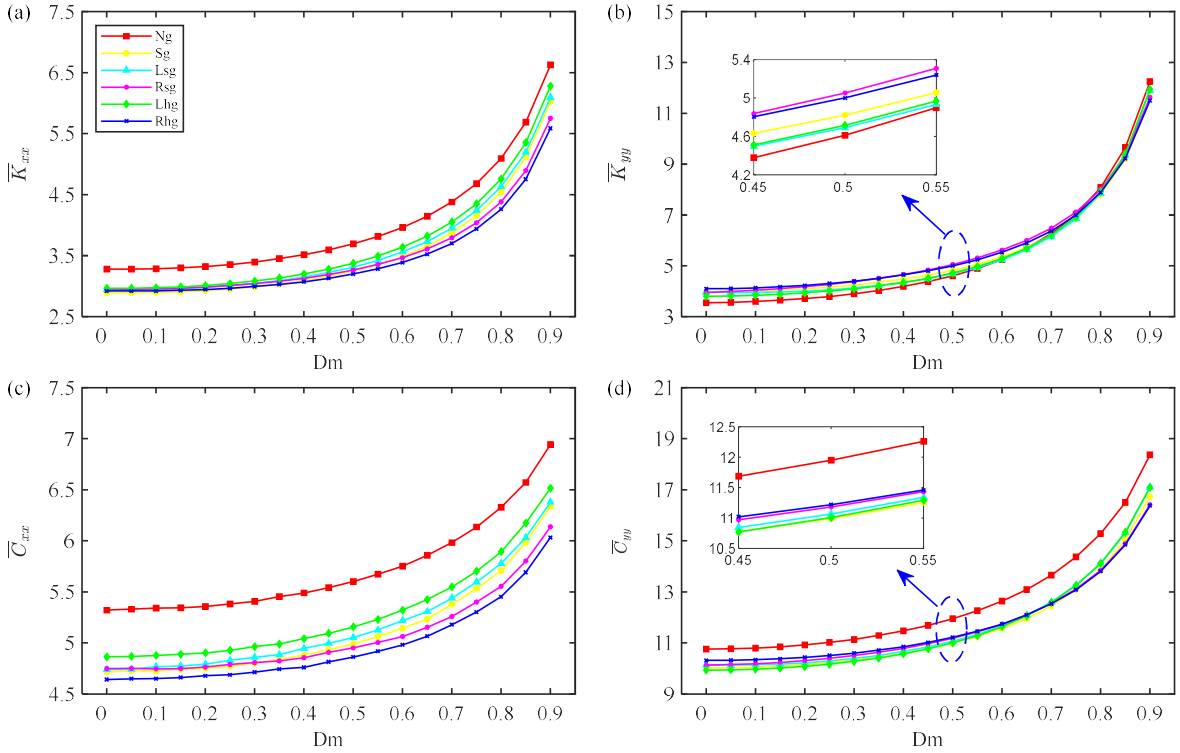

Figure 16. The effects of degree of misalignment on the dimensionless dynamic performance parameters of misaligned journal bearings under micro-grooves with different geometric shapes: (a) and (b) the main stiffness coefficients; (c) and (d) the main damping coefficients.

As shown in **Figure 16**, with the degree of misalignment increases, both the main stiffness coefficients and the main damping coefficients first increase slowly and then sharply. The K_{yy} of micro-grooves are greater than that of non-groove at a smaller degree of misalignment, and micro-groove significantly enhances the ability to resist external load in the y direction, while the other values of dynamic characteristics are smaller than that of non-groove. Under the chosen value of the degree of misalignment is 0.5, the dimensionless main stiffness coefficients K_{yy} of straight-groove, left spiral-groove, right spiral-groove, left herringbone-groove, and right herringbone-groove are decreased by 4.61%, 1.74%, 9.59%, 2.30%, and 8.46%, respectively, compared with that of no-grooved misaligned journal bearing. It can be seen that the static and dynamic characteristics of journal bearings with micro-grooves exhibits an obvious improvement at relatively small degree of misalignment, but this improvement weakens at a large degree of misalignment from the relative difference curve.

4.4.2. Effect of the misalignment angle

It should be pointed out that the variation of the misalignment angle ranges from 0° to 180° and the variation of the misalignment angle ranges from 180° to 360° are only different in direction and the values are the same, and then only the variation of the misalignment angle

ranges from 0° to 180° is displayed. The static and dynamic characteristic parameters of micro-grooved journal bearings with different misalignment angle are displayed respectively in **Figure 17** and **18**. As the misalignment angle increases, which is shown in **Figure 17**, the maximum fluid film pressure and the load carrying capacity decrease until the degree of 90° and then increases. An opposite trend is observed for the friction coefficient. The misalignment moment is greatest at 0° or 180° due to the maximum film pressure occurs on the front or rear end. Moreover, the misalignment moment slightly increases around 90° due to skewness is the largest in the full film region, and this phenomenon is consistent with the result of Jang and Khonsari[39]. As the misalignment angle increases, which is shown in **Figure 18**, the main stiffness coefficient K_{xx} and the main damping coefficient C_{xx} firstly increases and then decreases. The main stiffness coefficient K_{yy} and the main damping coefficient C_{yy} are similar to the trends of the load carrying capacity.

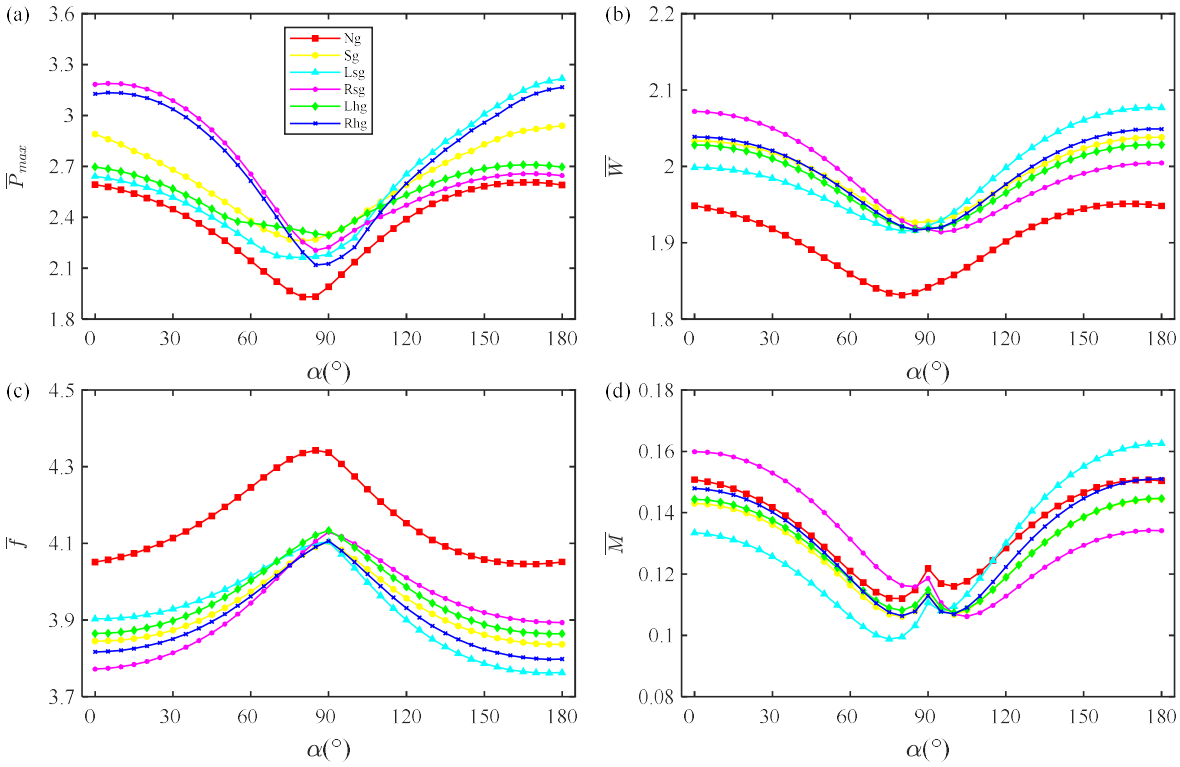

Figure 17. The effects of misalignment angle on the dimensionless static performance parameters of misaligned journal bearings under micro-grooves with different geometric shapes: (a) the maximum fluid pressure; (b) the load carrying capacity; (c) the friction coefficient; (d) the total misaligned moment.

It is found that the static and dynamic characteristics of the misaligned micro-grooved bearing show a significant improvement. Right spiral-groove has the best performance improvement for the bearing when the misalignment angle ranges from 0° to 90°, but the situation changes that left spiral-groove has the best performance improvement for the bearing beyond 90°. It can also be found that the micro-groove plays the positive role in increasing the load carrying capacity and the main stiffness coefficient K_{yy}, and reducing the friction coefficient, it is noted that the optimal geometric shape of the micro-groove changes when the misalignment angle exceeds 90°. The reason is that the fluid film pressure is not symmetrically distributed due to the journal misalignment, and maximum fluid film pressure occurs near at the front or rear end. Moreover, the variation of the misalignment angle leads to the variation of the inclined direction of the fluid film pressure, therefore, synchronously deflected micro-groove has the best performance improvement for the bearing.

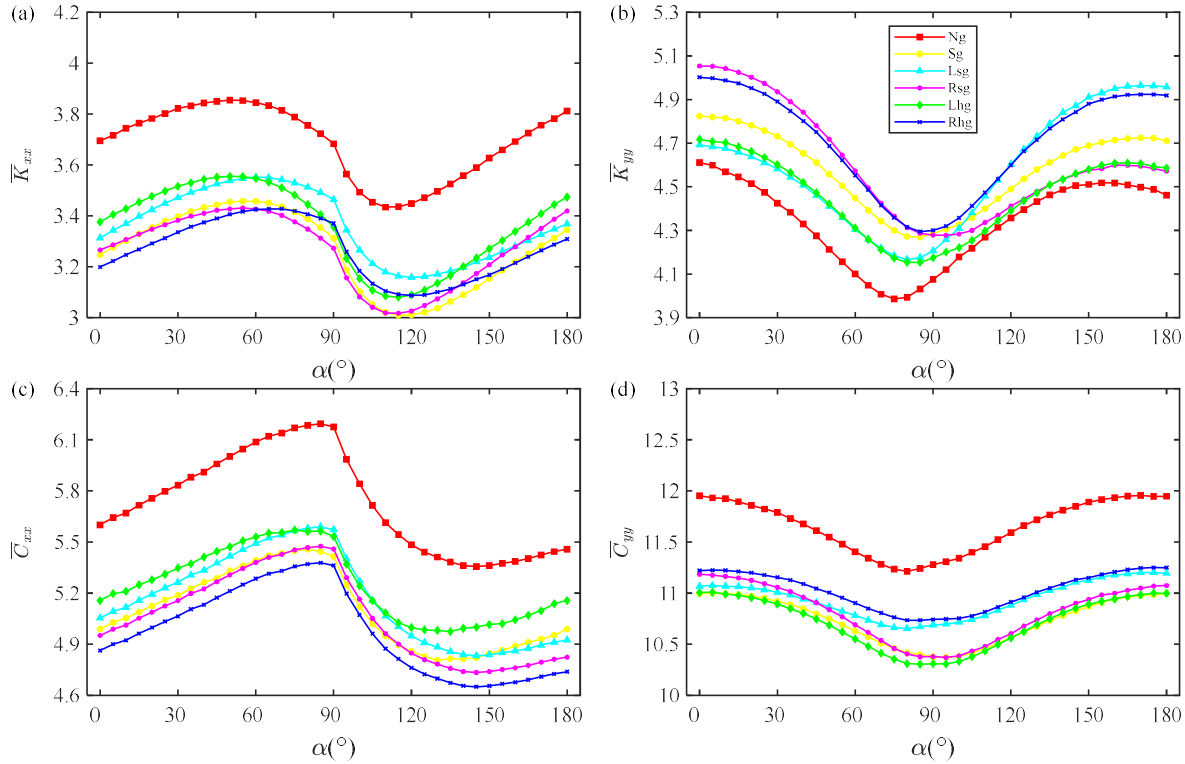

Figure 18. The effects of misalignment angle on the dimensionless dynamic performance parameters of misaligned journal bearings under micro-grooves with different geometric shapes: (a) and (b) the main stiffness coefficients; (c) and (d) the main damping coefficients.

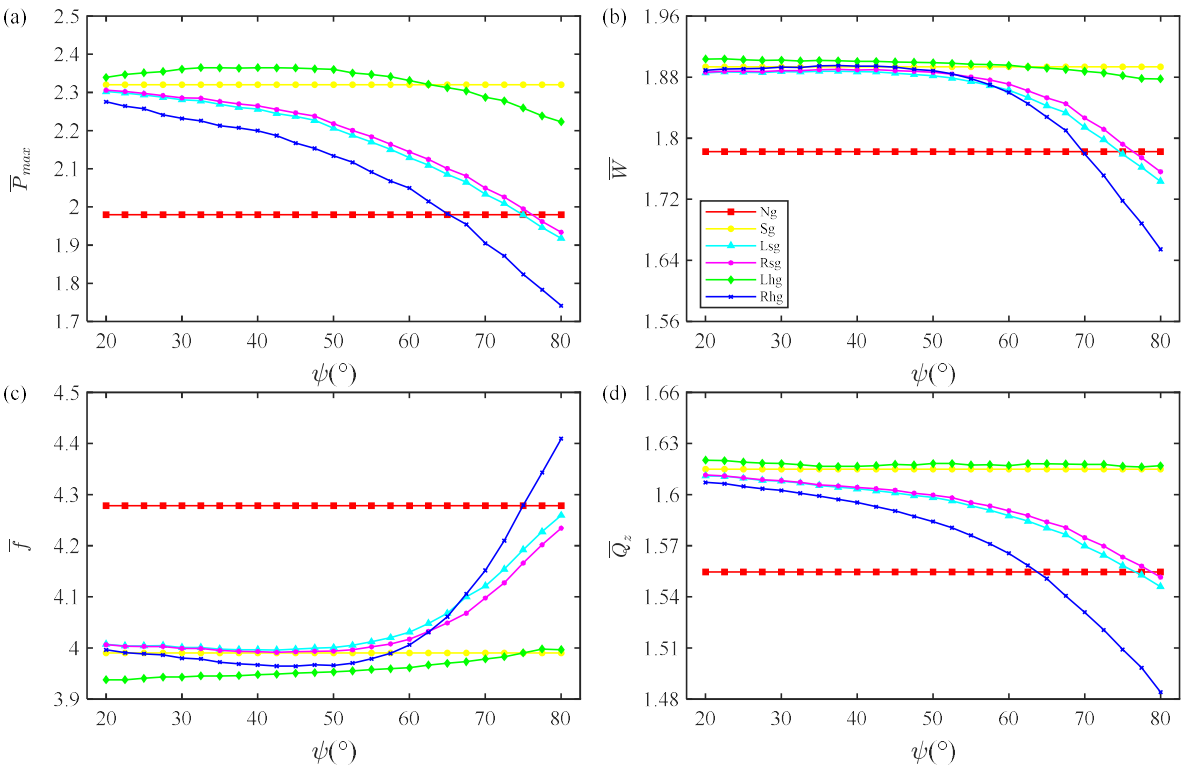

Figure 19. The effects of micro-groove deflection angle on the dimensionless static performance parameters of aligned journal bearings under micro-grooves with different geometric shapes: (a) the maximum fluid pressure; (b) the load carrying capacity; (c) the friction coefficient; (d) the side leakage flow rate.

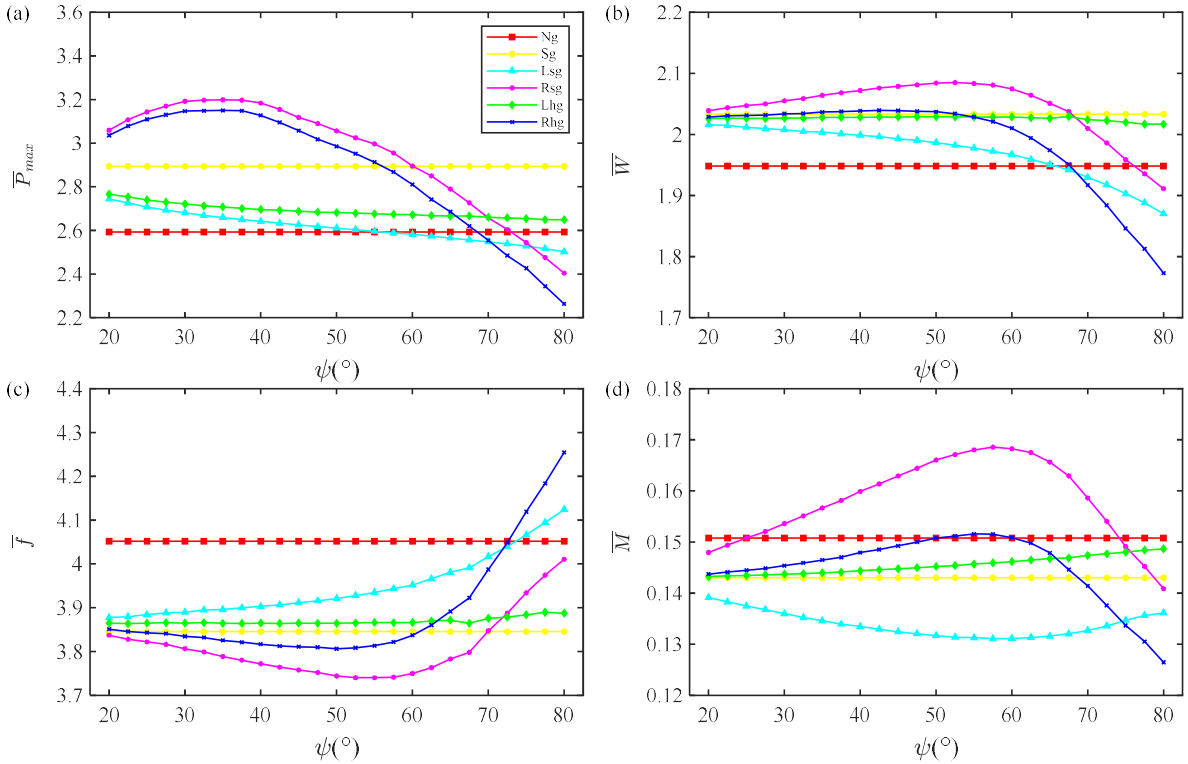

Figure 20. The effects of micro-groove deflection angle on the dimensionless static performance parameters of misaligned journal bearings under micro-grooves with different geometric shapes: (a) the maximum fluid pressure; (b) the load carrying capacity; (c) the friction coefficient; (d) the total misaligned moment.

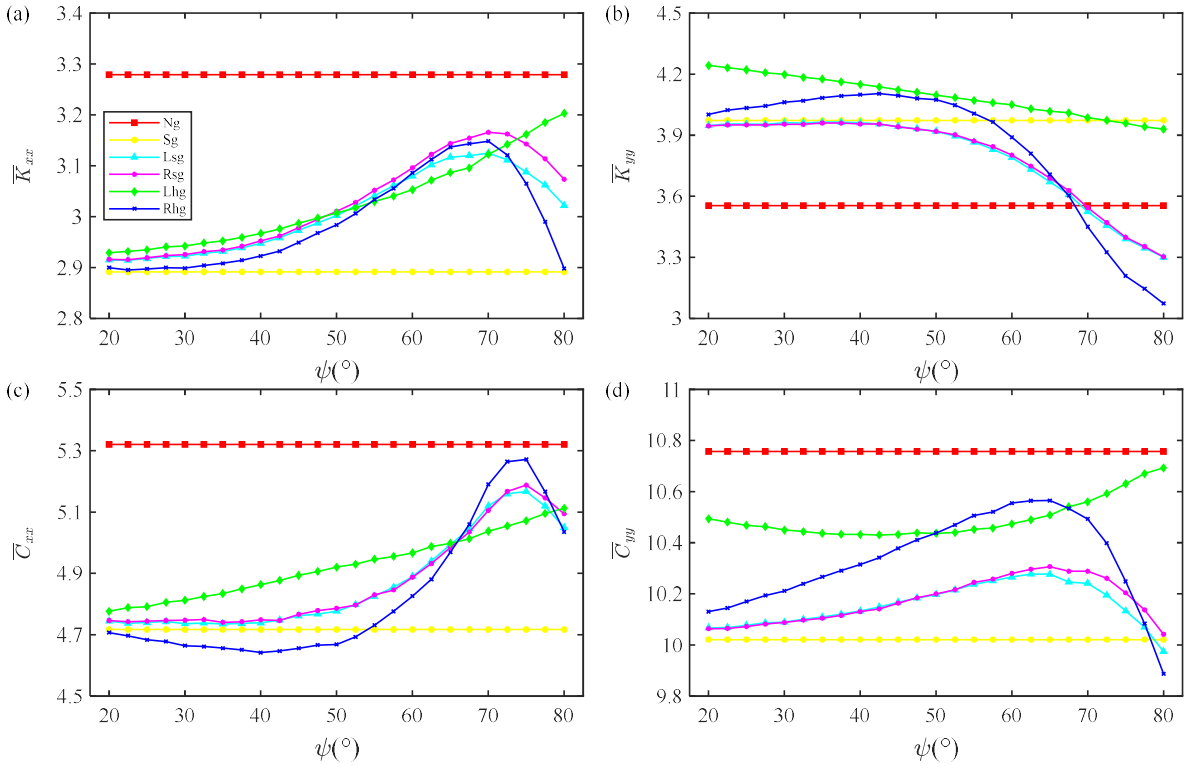

Figure 21. The effects of micro-groove deflection angle on the dimensionless dynamic performance parameters of aligned journal bearings under micro-grooves with different geometric shapes: (a) and (b) the main stiffness coefficients; (c) and (d) the main damping coefficients.

4.5. Effect of the micro-groove parameters

In this section, the effects of the micro-groove deflection angle and depth on the lubrication performance of aligned and misaligned micro-grooved journal bearings are analyzed. The micro-groove deflection angle ranging from 20° to 80° and the micro-groove dimensionless depth ranging from 0.1 to 0.5 are studied. The fluid film thickness at the front and rear ends changes due to journal misalignment, which in turn results in an asymmetric distribution of fluid film pressure.

4.5.1. Effect of the micro-groove deflection angle

The static characteristic parameters are displayed in **Figure 19** and **20**, and the dynamic characteristic parameters are displayed in **Figure 21** and **22**. It can be observed that the performance improvement of micro-grooved journal bearings with different geometric shapes are different with the micro-groove deflection angle increases. The optimal deflection angle of micro-groove is different for the aligned and misaligned journal bearings. Based on the research in the previous sections, it has been found that left herringbone-groove maximizes static and dynamic characteristics for aligned journal bearings, and right spiral-groove maximizes static and dynamic characteristics for misaligned journal bearings. Therefore, the purpose of this section is to find the optimal deflection angle of the micro-groove, so that the performances of the micro-grooved bearing can be improved to the best extent. The performance improvement is greatest for aligned journal bearing when the deflection angle of left herringbone-groove is 20°, and the performance improvement for misaligned journal bearings is greatest when the deflection angle of right spiral-groove is 55°.

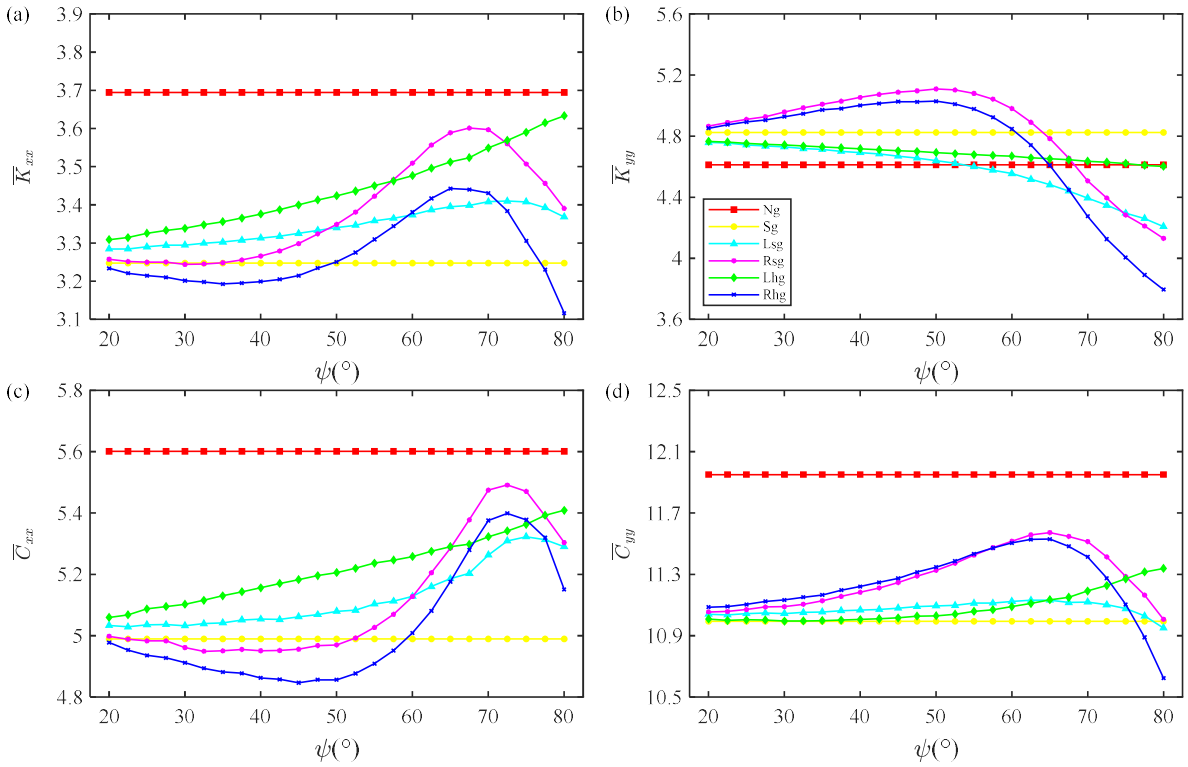

Figure 22. The effects of micro-groove deflection angle on the dimensionless dynamic performance parameters of misaligned journal bearings under micro-grooves with different geometric shapes: (a) and (b) the main stiffness coefficients; (c) and (d) the main damping coefficients.

Under the optimal value of micro-groove deflection angle is 20°, for the aligned journal bearing, the friction coefficients of straight-groove, left spiral-groove, right spiral-groove, left herringbone-groove, and right herringbone-groove are decreased by 6.74%, 6.34%, 6.36%,

7.96%, and 6.59%, respectively, compared with that of no-grooved journal bearing; the main stiffness coefficients K_{yy} of straight-groove, left spiral-groove, right spiral-groove, left herringbone-groove, and right herringbone-groove are decreased by 11.78%, 11.07%, 10.99%, 19.37%, and 12.59%, respectively, compared with that of no-grooved journal bearing. Under the optimal value of micro-groove deflection angle is 55°, for the misaligned journal bearing, the friction coefficients of straight-groove, left spiral-groove, right spiral-groove, left herringbone-groove, and right herringbone-groove are decreased by 5.09%, 2.88%, 7.69%, 4.58%, and 5.88%, respectively, compared with that of no-grooved journal bearing; the main stiffness coefficients K_{yy} of straight-groove, left spiral-groove, right spiral-groove, left herringbone-groove, and right herringbone-groove are decreased by 4.61%, -0.25%, 10.16%, 1.45%, and 7.93%, respectively, compared with that of no-grooved journal bearing. The main stiffness coefficient K_{yy} of the micro-grooved bearing is obviously larger than that of the non-grooved bearing at the optimal deflection angle, which is consistent with the analysis result of Yamada et al.[51]

4.5.2. Effect of the micro-groove depth

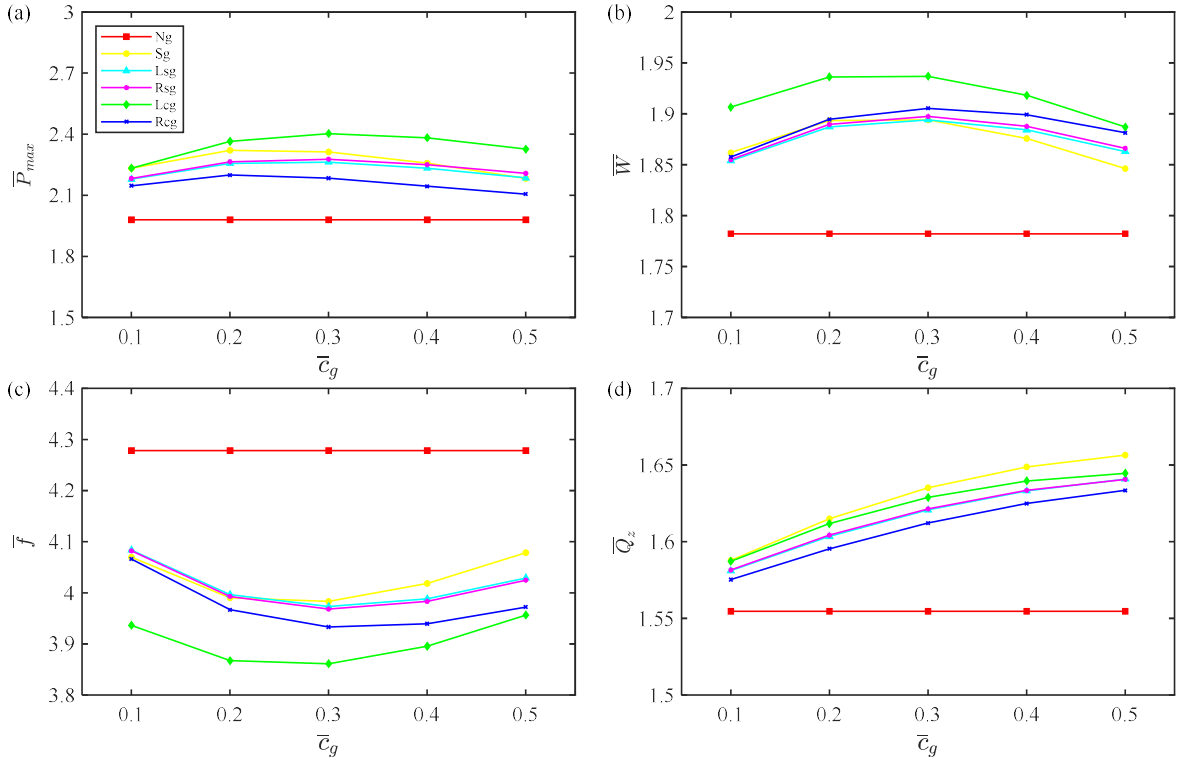

Figure 23. The effects of micro-groove depth on the dimensionless static performance parameters of aligned journal bearings under micro-grooves with different geometric shapes: (a) the maximum fluid pressure; (b) the load carrying capacity; (c) the friction coefficient; (d) the side leakage flow rate.

The static characteristic parameters are displayed in **Figure 23** and **24**, and the dynamic characteristic parameters are displayed in **Figure 25** and **26**. Analysis of the micro-groove depth similar to the deflection angle, there is also an optimal micro-groove depth. The purpose of this section is to find the optimal depth of the micro-groove, so that the performances of the micro-grooved bearing can be improved to the best extent. The performance improvement is greatest for aligned journal bearing when the dimensionless depth of left herringbone-groove is 0.2, and the performance improvement for misaligned journal bearings is greatest when the dimensionless depth of right spiral-groove is 0.2. Furthermore, as the micro-groove depth increases, resulting in the formation of the micro-

vortexes effect, there is an optimal micro-groove depth for the static and dynamic characteristics of the journal bearing.

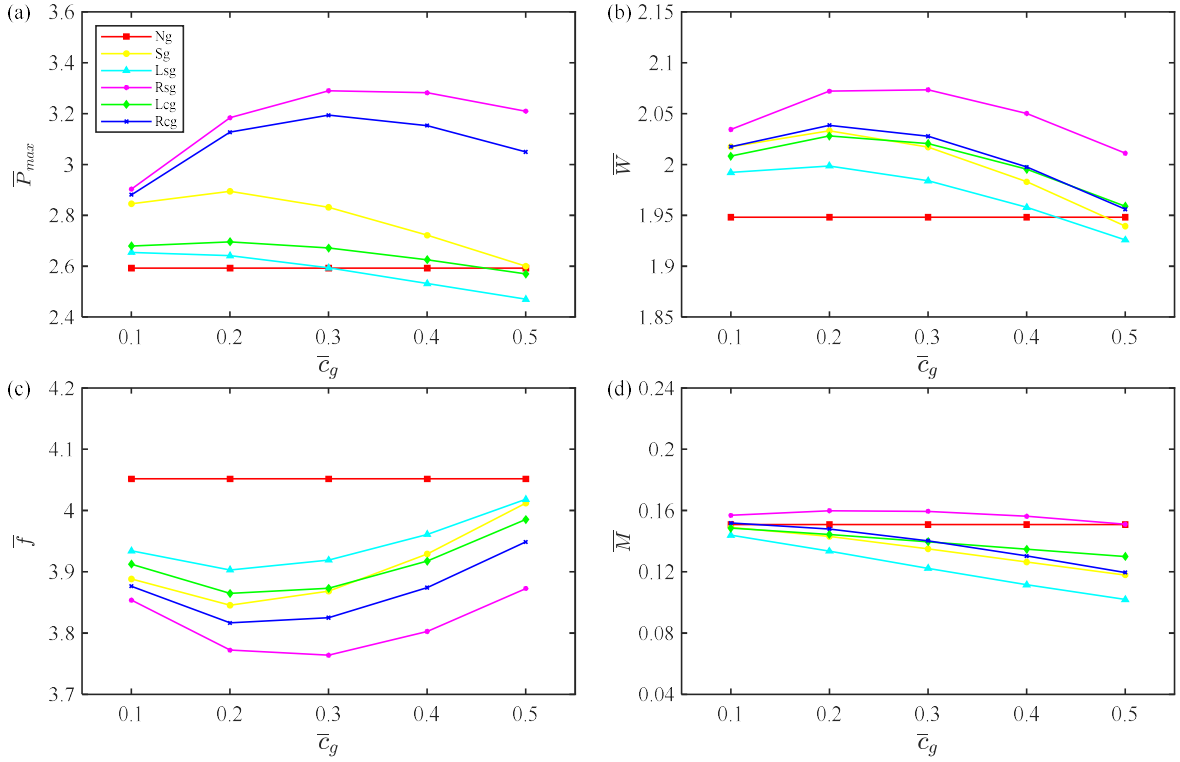

Figure 24. The effects of micro-groove depth on the dimensionless static performance parameters of misaligned journal bearings under micro-grooves with different geometric shapes: (a) the maximum fluid pressure; (b) the load carrying capacity; (c) the friction coefficient; (d) the total misaligned moment.

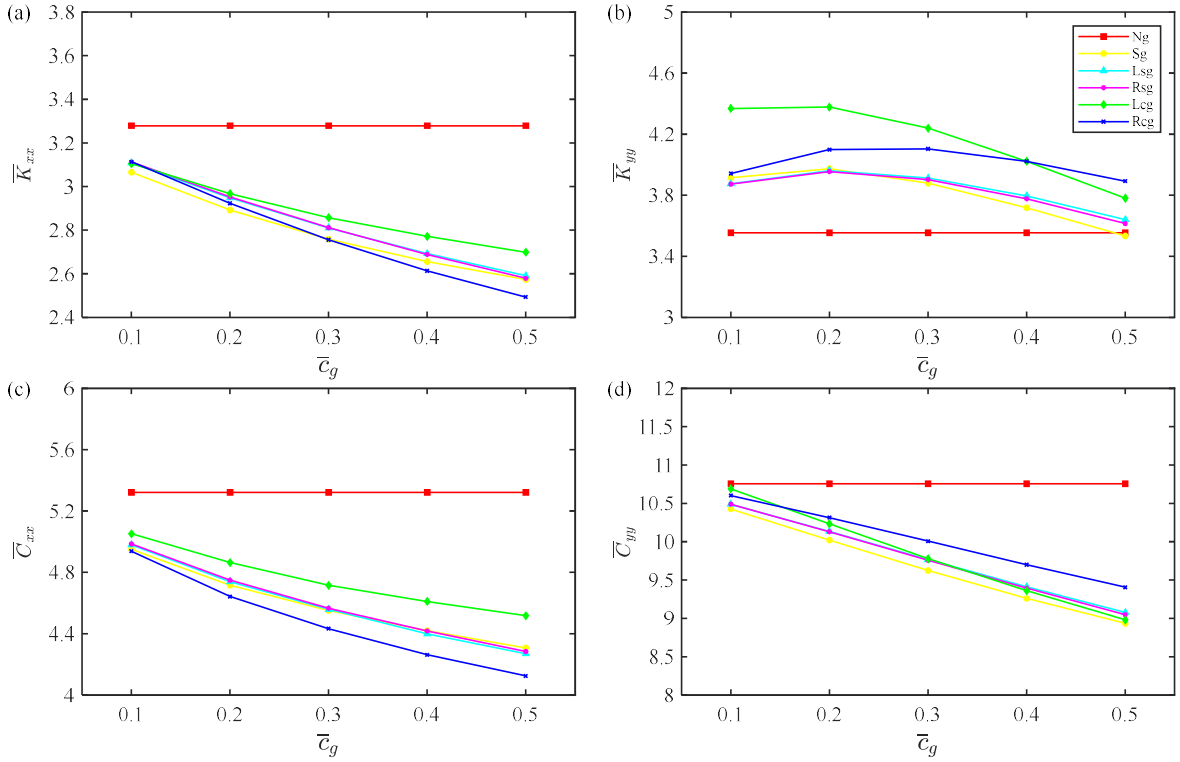

Figure 25. The effects of micro-groove depth on the dimensionless dynamic performance parameters of aligned journal bearings under micro-grooves with different geometric shapes: (a) and (b) the main stiffness coefficients; (c) and (d) the main damping coefficients.

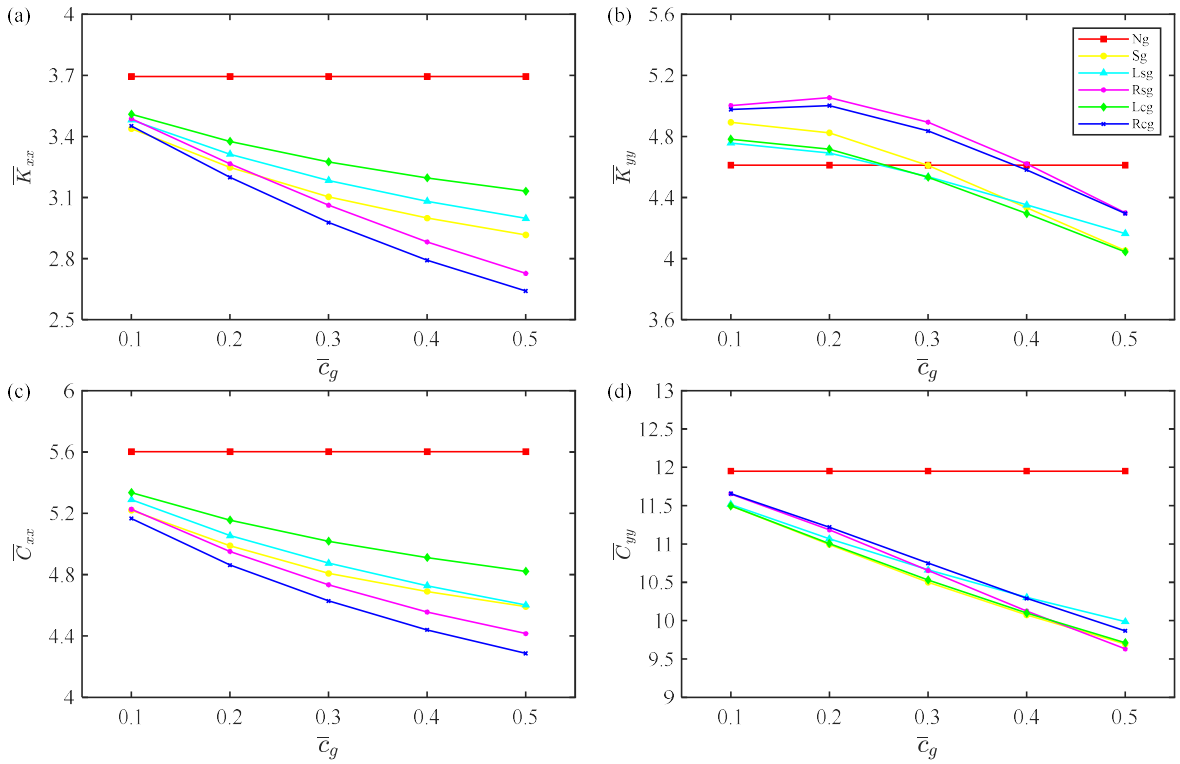

Figure 26. The effects of micro-groove depth on the dimensionless dynamic performance parameters of misaligned journal bearings under micro-grooves with different geometric shapes: (a) and (b) the main stiffness coefficients; (c) and (d) the main damping coefficients.

Under the optimal value of micro-groove dimensionless depth is 0.2, for the aligned journal bearing, the friction coefficients of straight-groove, left spiral-groove, right spiral-groove, left herringbone-groove, and right herringbone-groove are decreased by 6.74%, 6.58%, 6.67%, 9.61%, and 7.28%, respectively, compared with that of no-grooved journal bearing; the main stiffness coefficients K_{yy} of straight-groove, left spiral-groove, right spiral-groove, left herringbone-groove, and right herringbone-groove are decreased by 11.78%, 11.44%, 11.28%, 23.17%, and 15.32%, respectively, compared with that of no-grooved journal bearing. Under the optimal value of micro-groove dimensionless depth is also 0.2, for the misaligned journal bearing, the friction coefficients of straight-groove, left spiral-groove, right spiral-groove, left herringbone-groove, and right herringbone-groove are decreased by 5.09%, 3.66%, 6.90%, 4.61%, and 5.80%, respectively, compared with that of no-grooved journal bearing; the main stiffness coefficients K_{yy} of straight-groove, left spiral-groove, right spiral-groove, left herringbone-groove, and right herringbone-groove are decreased by 4.61%, 1.74%, 9.59%, 2.30%, and 8.46%, respectively, compared with that of no-grooved journal bearing.

5. Conclusions

In this paper, a modified lubrication model considering micro-groove and misalignment of journal bearing is proposed to study the effects of eccentricity ratio, misalignment (degree of misalignment and misalignment angle) and micro-groove parameters (micro-groove geometric shape, deflection angle and depth) on the static and dynamic characteristics of journal bearings. An average Reynolds equation that satisfies the mass-conserving cavitation algorithm considering fluid film rupture and reformation is developed. Furthermore, the hydrodynamic lubrication characteristics of micro-grooved bearings between models with and without misalignment are compared numerically. Based on the numerical analysis, the relevant conclusions obtained are drawn as follows:

(1) Under relatively small eccentricity ratio, micro-grooved with reasonable parameter have the positive effect on the lubrication performance of bearing, such as, the load carrying capacity and the main stiffness coefficient K_{yy} significantly increase, the friction coefficient reduces, and the ability to resist external load enhanced. The hydrodynamic effect is more pronounced as the eccentricity ratio increases, however the ability of the micro-groove to improve the performance of bearings is gradually weakened.
(2) The journal misalignment changes the distribution of the fluid film at the front and rear ends, and reducing the minimum fluid film thickness. As the degree of misalignment increases, the load carrying capacity, main stiffness and damping coefficients increase, the friction coefficient decreases under the same eccentricity ratio. While the misalignment angle has a opposite effect on the performance characteristics of journal bearing. Additionally, the static and dynamic characteristics of bearing are improved obviously when degree of misalignment is smaller and misalignment angle is 0° or 180°.
(3) The geometric shape, deflection angle and depth of micro-groove play the decisive role in the bearing performance improvement. Under the optimal deflection angle and depth, the left herringbone-grooved bearing surface provides the superior lubrication characteristics of aligned journal bearings compared with other micro-grooved bearing surfaces, while the right spiral-grooved bearing surface provides the superior lubrication characteristics of misaligned journal bearings compared with other micro-grooved bearing surfaces.

In summary, the present work shows that the micro-groove parameters can be reasonably selected according the actual working conditions, thereby improving the lubrication performance of journal bearings. The optimum parameters of the micro-groove are dependent on the operating conditions of journal bearings. In the future work, the influence factors of the temperature and air content of lubricant will be considered to further analyze the lubrication performance of journal bearing to prolong the service life.

Acknowledgements

The authors would like to thank anonymous reviewers and editor for their constructive suggestions, which helped to improve the quality of this article.

Declaration of conflicting interests

The authors declared no potential conflicts of interest with respect to the research, authorship, and/or publication of this article.

Funding

The authors disclosed receipt of the following financial support for the research, authorship, and/or publication of this article: This study was supported by the National Natural Science Foundation of China (Nos. 52175085 and 51875166).

ORCID iDs

Peng Li: https://orcid.org/0000-0002-6487-0705
Hao Zhang: https://orcid.org/0000-0002-1327-1091

References

1. Mallya R, Shenoy SB and Pai R. Static characteristics of misaligned multiple axial groove water-lubricated bearing in the turbulent regime. *Proc IMechE, Part J: J Engineering Tribology* 2017; 231: 385-398.
2. Shi JH, Cao HR and Chen XF. Effect of angular misalignment on the dynamic characteristics of externally pressurized air journal bearing. *Proc IMechE, Part J: J Engineering Tribology* 2019; 234: 205-228.
3. Jang JY and Khonsari MM. On the wear of dynamically-loaded engine bearings with provision for misalignment and surface roughness. *Tribol Int* 2020; 141: 105919.

4. Xiang G, Yang TY, Guo J, et al. Optimization transient wear and contact performances of water-lubricated bearings under fluid-solid-thermal coupling condition using profile modification. *Wear* 2022; 502-503: 204379.
5. MaKee SA and McKee TR. Pressure distribution in the oil film of journal bearings. *J Tribol* 1932; 54: 14-65.
6. Dubois GB, Mabie HH and Ocvirk FW. Experimental investigation of oil film pressure distribution for misaligned plain bearings, national advisory committee for aeronautic. *NACA Technical Note 3352* 1951.
7. Sun J and Gui CL. Hydrodynamic lubrication analysis of journal bearing considering misalignment caused by shaft deformation. *Tribol Int* 2004; 37: 841-848.
8. Sun J, Gui CL, Li ZY, et al. Influence of journal misalignment caused by shaft deformation under rotational load on performance of journal bearing. *Proc IMechE, Part J: J Engineering Tribology* 2005; 219: 275-283.
9. Lv FR, Ta N and Rao ZS. Analysis of equivalent supporting point location and carrying capacity of misaligned journal bearing. *Tribol Int* 2017; 116: 26-38.
10. Feng HH, Jiang SY and Ji AM. Investigations of the static and dynamic characteristics of water-lubricated hydrodynamic journal bearing considering turbulent, thermohydrodynamic and misaligned effects. *Tribol Int* 2019; 130: 245-260.
11. Zheng LY, Zhu HH, Zhu, JC, et al. Effects of oil film thickness and viscosity on the performance of misaligned journal bearings with couple stress lubricants. *Tribol Int* 2020; 146: 106229.
12. El-Butch AM and Ashour NM. Transient analysis of misaligned elastic tilting-pad journal bearing. *Tribol Int* 2005; 38: 41-48.
13. Wang YS, Wang QJ and Lin C. A mixed-EHL analysis of effects of misalignments and elastic deformations on the performance of a coupled journal-thrust bearing system. *Tribol Int* 2006; 39: 281-289.
14. Guha SK. Analysis of steady-state characteristics of misaligned hydrodynamic journal bearings with isotropic roughness effect. *Tribol Int* 2000; 33: 1-12.
15. Meng FM, Wang Q, Hua D and Liu J. A simple method to calculate contact factor used in average flow model. *J Tribol* 2010; 132: 269-272.
16. Meng FM, Wang WZ, Hu YZ and Wang H. Numerical analysis of combined influences of inter-asperity cavitation and elastic deformation on flow factors. *Proc IMechE, Part C: J Mechanical Engineering Science* 2007; 221: 815-827.
17. Meng FM, Qing DT, Hu YZ and Wang H. Study on combined influence of inter-asperity cavitation and elastic deformation of non-Gaussian surface on flow factors. Proceedings of the Institution of Mechanical Engineers. *Proc IMechE, Part C: J Mechanical Engineering Science* 2008; 222: 1039-1048.
18. Meng FM, Cen SQ, Hu YZ and Wang H. On elastic deformation, inter-asperity cavitation and lubricant thermal effects on flow factors. *Tribol Int* 2009; 42: 260-274.
19. Lv FR, Rao ZS, Ta N, et al. Mixed-lubrication analysis of thin polymer film overplayed metallic marine stern bearing considering wall slip and journal misalignment. *Tribol Int* 2017; 109: 390-397.
20. Lv FR, Jiao CX, Ta N, et al. Mixed-lubrication analysis of misaligned bearing considering turbulence. *Tribol Int* 2018; 119: 19-26.
21. Zhu SY, Sun J, Li B, et al. Thermal turbulent lubrication analysis of rough surface journal bearing with journal misalignment. *Tribol Int* 2020; 144: 106109.
22. Xie ZL, Shen NW, Zhu WD, et al. Theoretical and experimental investigation on the influences of misalignment on the lubrication performances and lubrication regimes transition of water lubricated bearing. *Mech Syst Sig Process* 2021; 149: 107211.
23. Ma JJ, Fu C, Zhang H, et al. Modelling non-Gaussian surfaces and misalignment for condition monitoring of journal bearings. *Measurement* 2021; 174: 108983.
24. Sahu K, Sharma SC and Ram N. Misalignment and surface irregularities effect in MR fluid journal bearing. *Int J Mech Sci* 2022; 221: 107196.
25. Gropper D, Wang L and Harvey TJ. Hydrodynamic lubrication of textured surfaces: a review of modeling techniques and key findings. *Tribol Int* 2016; 94: 509-529.
26. Adatepe H, Bıyıklıoglu A and Sofuoglu H. An investigation of tribological behaviors of dynamically loaded non-grooved and micro-grooved journal bearings. *Tribol Int* 2013; 58: 12-19.
27. Adatepe H, Bıyıklıoglu A and Sofuoglu H. An experimental investigation on frictional behavior of statically loaded micro-grooved journal bearing. *Tribol Int* 2011; 44: 1942-1948.
28. Kango S, Sharma RK and Pandey RK. Comparative analysis of textured and grooved hydrodynamic journal bearing. *Proc IMechE, Part J: J Engineering Tribology* 2013; 228: 82-95.
29. Miyanaga N and Tomioka J. Effect of support stiffness and damping on stability characteristics of herringbone-grooved aerodynamic journal bearings mounted on viscoelastic supports. *Tribol Int* 2016; 100: 195-203.
30. Gong JY, Jin Y, Liu ZL, et al. Study on influencing factors of lubrication performance of water-lubricated micro-groove bearing. *Tribol Int* 2019; 129: 390-397.

31. Xiang G and Han YF. Study on the tribo-dynamic performance of water-lubricated microgroove bearings during start-up. *Tribol Int* 2020; 151: 106395.
32. Chen SA, Xiang G, Fillon M, et al. On the tribo-dynamic behaviors during start-up of water lubricated bearing considering imperfect journal. *Tribol Int* 2022; 174: 107685.
33. Cai JL, Xiang G, Li S, et al. Mathematical modeling for nonlinear dynamic mixed friction behaviors of novel coupled bearing lubricated with low-viscosity fluid. *Phys. Fluids* 2022; 34: 093612.
34. Cai JL, Han YF, Xiang G, et al. Influence of the mass conservation cavitation boundary on the tribo-dynamic responses of the micro-groove water-lubricated bearing. *Surf. Topogr.: Metrol. Prop.* 2022; 10: 045011.
35. Xie ZL, Wang XR and Zhu WD. Theoretical and experimental exploration into the fluid structure coupling dynamic behaviors towards water-lubricated bearing with axial asymmetric grooves. *Mech Syst Sig Process* 2022; 168: 108624.
36. Shen C and Khonsari MM. Numerical optimization of texture shape for parallel surfaces under unidirectional and bidirectional sliding. *Tribol Int* 2015; 82: 1-11.
37. Shinde AB and Pawar PM. Multi-objective optimization of surface textured journal bearing by Taguchi based Grey relational analysis. *Tribol Int* 2017; 114: 349-357.
38. Patir N and Cheng HS. An average flow model for determining effects of three-dimensional roughness on partial hydrodynamic lubrication. *J Lubr Technol* 1978; 100: 12-17.
39. Patir N and Cheng HS. Application of average flow model to lubrication between rough sliding surfaces. *J Lubr Technol* 1979; 101, 220-229.
40. Wu CW and Zheng LQ. An average Reynolds equation for partial film lubrication with a contact factor. *J Tribol* 1989; 111: 188-191.
41. Jang JY and Khonsari MM. On the behavior of misaligned journal bearings based on mass-conservative thermohydrodynamic analysis. *J Tribol* 2010; 132: 011702.
42. Ausas R, Ragot P, Leiva J, et al. The impact of the cavitation model in the analysis of microtextured lubricated journal bearings. *J Tribol* 2007; 129: 868-875.
43. Profito FJ, Vlădescu SC, Reddyhoff T and Dini D. Transient experimental and modelling studies of laser-textured micro-grooved surfaces with a focus on piston-ring cylinder liner contacts. *Tribol Int* 2017; 113: 125-136.
44. Greenwood JA and Tripp JH. The contact of two nominally flat rough surfaces. *Proc IMechE, Part J: J Engineering Tribology* 1970; 185: 625-634.
45. Liang P, Li XY, Guo F, et al. Influence of sea wave shock on transient start-up performance of water-lubricated bearing. *Tribol Int* 2022; 167: 107332.
46. Zhou GW, Qiao JS, Pu W, et al. Analysis of mixed lubrication performance of water-lubricated rubber tilting pad journal bearing. *Tribol Int* 2022; 169: 107423.
47. Jang JY and Khonsari MM. Performance and characterization of dynamically-loaded engine bearings with provision for misalignment. *Tribol Int* 2019; 130: 387-399.
48. Wang XK, Zhou L, Huang M, et al. Numerical investigation of journal misalignment on the static and dynamic characteristics of aerostatic journal bearings. *Measurement* 2018; 128: 314-324.
49. Li P, Zeng F, Xiao S, et al. Effects of texture bottom profile on static and dynamic characteristics of journal bearings. *Shock Vib* 2021; 7068744.
50. Zhang ZM, Zhang YY, Xie YB, et al. *Fluid dynamic lubrication theory of sliding bearings*. Beijing: Advanced Education Press, 1986.
51. Meng FM, Zhang YF, Su LL, et al. Dynamic characteristics of compound textured journal bearing. *Proc IMechE, Part J: J Engineering Tribology* 2020; 235: 1312-1334.
52. Yamada H, Taura H and Kaneko S. Numerical and experimental analyses of the dynamic characteristics of journal bearings with square dimples. *J Tribol* 2018; 140: 011703.

Appendix

Notation

c	radial clearance, mm
R	bearing radius, mm
r	journal radius, mm
L	bearing width, mm
e	eccentricity, mm
e'	misalignment eccentricity, mm
ε	eccentricity ratio

ε'	misalignment eccentricity ratio
$\varepsilon'_{\max}$	maximum misalignment eccentricity ratio
D_m	degree of misalignment
x, y,z	coordinate system of journal bearing
φ	circumferential coordinate
Z	axial coordinate
$h / h_{\min}$	nominal/minimum film thickness, mm
$p_\varsigma / p_{\max}$	fluid pressure/maximum pressure, Pa
Θ	cavitation fraction
u	circumferential velocity of journal, $m \cdot s^{-1}$
t	time, s
ϕ_x, ϕ_z	pressure flow factors
ϕ_s	shear flow factor
ϕ_c	contact factor
p_{asp}	contact pressure, Pa
μ_{dry}	dry friction coefficient
σ_j, σ_b	surface roughness parameter, μm
σ	combined surface roughness, μm
υ_b, υ_j	Poisson ratio of bearing and journal
E_b, E_j	elastic modulus of bearing and journal, GPa
E^*	composite elastic modulus, GPa
T_{shell}	thickness of bearing shell, mm
ν_0	equivalent Poisson's ratio
h_g	film thickness of micro-groove, μm
c_x	micro-groove length, mm
c_z	micro-groove width, mm
c_g	micro-groove depth, μm
ψ	deflection angle of micro-groove, deg
W	load carrying capacity, N
F	frictional force, N
f	friction coefficient
Q_z	side leakage flow rate, $m^3 \cdot s^{-1}$
M	total misaligned moment, N·m
ϕ_M	moment direction angle, rad
k_{ij}	fluid film stiffness coefficients, $N \cdot m^{-1}$
c_{ij}	fluid film damping coefficients, $N \cdot s \cdot m^{-1}$

Dimensionless parameters

$\bar{h} / \bar{h}_{\min}$	$\left(h / h_{\min}\right) / c$
$\bar{\sigma}$	σ / c

$\overline{\delta}$	δ/c
$\overline{u}$	u/U
$\overline{t}$	$t/(R/U)$
$\overline{P}_{\varsigma}/\overline{P}_{\max}$	$(p_{\varsigma}/p_{\max})/(\mu UR/c^2)$
$\overline{W}$	$W/(\mu UR^2L/c^2)$
$\overline{F}$	$F/(\mu URL/c)$
$\overline{Q}_z$	$Q_z/(cUR^2/L)$
$\overline{M}$	$M/(\mu UR^2L^2/c^2)$
K_{ij}	$k_{ij}/(\mu UR^2L/c^3)$
C_{ij}	$c_{ij}/(\mu UR^2L/c^3\omega)$

Greek symbols

α	misalignment angle, deg
ρ	fluid density, Kg·m^{-3}
μ	fluid viscosity, Pa·s
ω	rotation speed of journal, rpm
γ	roughness directions
β	curvature radius asperities, μm
η	density of asperities, μm^{-2}
θ	attitude angle, deg
δ	elastic deformation of bearing shell, μm

Superscripts and subscripts

–	dimensionless term
b, *j*	bearing, journal
max/ min	maximum/minimum dimension
0	steady-state condition